Diverse collective excitations in ^{159}Er up to high spin

M. Mustafa,[1] J. Ollier,[2] J. Simpson,[2,*] M. A. Riley,[3] E. S. Paul,[1] X. Wang,[3] A. Aguilar,[3] M. P. Carpenter,[4] I. G. Darby,[5,†] D. J. Hartley,[6] R. V. F. Janssens,[4] F. G. Kondev,[7] T. Lauritsen,[4] P. J. Nolan,[1] M. Petri,[1,‡] J. M. Rees,[1] J. P. Revill,[1] S. V. Rigby,[1] C. Teal,[3] J. Thomson,[1] C. Unsworth,[1] S. Zhu,[4] B. G. Carlsson,[8] H. L. Ma,[8,§] T. Mufti,[8] and I. Ragnarsson[8]

[1]*Oliver Lodge Laboratory, University of Liverpool, Liverpool L69 7ZE, United Kingdom*
[2]*STFC Daresbury Laboratory, Daresbury, Warrington WA4 4AD, United Kingdom*
[3]*Department of Physics, Florida State University, Tallahassee, Florida 32306, USA*
[4]*Physics Division, Argonne National Laboratory, Argonne, Illinois 60439, USA*
[5]*Department of Physics and Astronomy, University of Tennessee, Knoxville, Tennessee 37996, USA*
[6]*Department of Physics, U.S. Naval Academy, Annapolis, Maryland 21402, USA*
[7]*Nuclear Engineering Division, Argonne National Laboratory, Argonne, Illinois 60439, USA*
[8]*Division of Mathematical Physics, LTH, Lund University, Post Office Box 118, S-22100 Lund, Sweden*

(Received 12 October 2011; published 22 November 2011)

A spectroscopic investigation of the γ decays from excited states in ^{159}Er has been performed to study the changing structural properties exhibited as ultrahigh spins ($I > 60\hbar$) are approached. The nucleus of ^{159}Er was populated by the reaction ^{116}Cd(^{48}Ca,$5n\gamma$) at a beam energy of 215 MeV, and the resulting γ decays were studied using the Gammasphere spectrometer. New rotational bands and extensions to existing sequences were observed, which are discussed in terms of the cranked shell model, revealing a diverse range of quasiparticle configurations. At spins around $50\hbar$, there is evidence for a change from dominant prolate collective motion at the yrast line to oblate non-collective structures via the mechanism of band termination. A possible strongly deformed triaxial band occurs at these high spins, which indicates collectivity beyond $50\hbar$. The high-spin data are interpreted within the framework of cranked Nilsson-Strutinsky calculations.

DOI: 10.1103/PhysRevC.84.054320 PACS number(s): 27.70.+q, 21.10.Re, 23.20.Lv

I. INTRODUCTION

The study of nuclear structure toward the extremes of angular momentum has been at the forefront of γ-ray spectroscopy since its inception. Pushing to such extremes tests theoretical models to their limits. The diverse nature of collective motion in the rare-earth nuclei around $A = 160$ at high spin makes this mass region an excellent testing ground for such models that attempt to explain the deformed nuclear shapes that they exhibit and their behavior in terms of the underlying single-particle configurations. An example of this diverse nature is the observation that collective rotational bands appear to terminate at discrete states around spin $40\hbar$ in nuclei with $N \sim 90$ [1–11]. This has been interpreted as a dramatic change in structure from a collective prolate shape to an oblate single-particle shape via the mechanism of band termination [12,13]. This phenomenon occurs when the spin vectors of the available valence nucleons outside a closed-shell core, in this case $^{146}_{64}$Gd$_{82}$, become aligned in pure single-particle configurations [13]. In the $N = 90$ nucleus of ^{158}Er, such single-particle states are observed at $I^\pi = 40^+$ [1] and 46^+ [2] in the yrast (lowest energy for a given spin) band and at43^-, 48^-, and 49^- [14] in the lowest-energy negative-parity sequences. Moreover, rotational sequences have recently been identified that extend into the region of ultrahigh spin ($> 60\hbar$) [15] and represent a reemergence of collectivity beyond band termination in ^{158}Er. Comparison with results from cranked Nilsson-Strutinsky (CNS) calculations suggests that these collective rotational sequences are based on triaxial strongly deformed (TSD) shapes, although uncertainties persist as to the exact value of the γ deformation [16]. A number of similar collective structures with characteristic high moments of inertia have now been observed in several neighboring nuclei [17–21].

The present paper reports on a detailed spectroscopic investigation of ^{158}Er's odd-neutron neighbor $^{159}_{68}$Er$_{91}$. Previous experimental papers have identified a number of rotational bands based on the odd neutron, which resides in a variety of quasiparticle configurations [22–26], discussed within the framework of the cranked shell model [27,28]. Evidence for the onset of a transition from collective rotation to an oblate single-particle shape in the yrast band at $\sim 50\hbar$ was discussed in Refs. [24,26]. A further feature was observed at high spin in the band based on the negative-parity ground-state configuration [24], which has been interpreted as an unpaired neutron-band crossing [29]. This is a crossing that occurs in the absence of static neutron-pairing correlations. In the present paper, new rotational bands have been observed in ^{159}Er, and significant extensions to existing ones have been made. These results are interpreted within the framework of the cranked shell model. Also, a new band based on a γ-vibrational excitation is discussed. In addition, a terminating state at $I^\pi = 101/2^+$ and evidence for terminating structures close to the yrast states in various bands at spins around $\sim 50\hbar$ have

*john.simpson@stfc.ac.uk
†Present address: IAEA Nuclear Spectrometry and Applications Laboratory, Physics Section, A-2444, Siebersdorf, Austria.
‡Present address: Nuclear Science Division, Lawrence Berkeley National Laboratory, Berkeley, CA 94720.
§Permanent address: China Institute of Atomic Energy, P.O. Box 275-10, Beijing 102413, China.

been identified. CNS calculations have been performed to help understand the underlying configurations of these high-spin sequences. Good agreement between experiment and theory is observed for the competition of the prolate-collective and band-terminating sequences in the $I = 30 - 50\hbar$ region. The present experiment has also identified a band with a high moment of inertia, which is discussed in terms of a strongly deformed triaxial structure [20]. The lifetimes of states within similar structures in ^{157,158}Er [16] indicate discrepancies between the experimentally deduced and the predicted triaxial shapes. The implications of this observation for ^{159}Er are discussed.

II. EXPERIMENTAL DETAILS

The experiment was performed by using the ATLAS facility at Argonne National Laboratory. Excited states in ^{159}Er were populated by using a 215-MeV beam of ^{48}Ca, incident upon enriched (98.7%) targets of ^{116}Cd, which induced fusion-evaporation reactions. The target was composed of two self-supporting ^{116}Cd foils with a total thickness of 1.3 mg/cm^2. The γ decays, which result from the reaction products, were detected by using the Gammasphere γ-ray spectrometer [30,31]. A total of $\sim 1.9 \times 10^9$ events were collected when, at least, 7 of the 101 Compton-suppressed high-purity germanium detectors fired in prompt coincidence. The data were collected over a 5-day period. Unfolding the events resulted in approximately 1.4×10^{11} triple and 3.5×10^{10} quadruple coincidence events. These were replayed off-line into RadWare-format three-dimensional (E_γ^3) cubes [32] and four-dimensional (E_γ^4) hypercubes [33] for analysis.

One-dimensional spectra were also unfolded directly from the data by using the technique discussed in Ref. [34]. They were produced with multiple gates set on inband stretched quadrupole ($E2$) transitions from ^{159}Er up to fold five (γ^5) where the data were separated further into the corresponding detectors in the rings of the Gammasphere at a fixed angle θ to the beam direction. Then, angle-specific spectra were analyzed to obtain angular-intensity ratios and, based on the method of directional correlations from oriented states [35], were used to determine γ-ray multipolarities. The ratio R of the intensity of transitions at $\sim 130^\circ(50^\circ)$ and 90° to the beam direction was measured and was given by

$$R = \frac{I_\gamma[\theta \sim 130^\circ(50^\circ)]}{I_\gamma[\theta \sim 90^\circ]}. \quad (1)$$

This ratio is approximately a factor of 2 larger for stretched quadrupole ($\Delta I = 2$) and pure nonstretched dipole transitions ($\Delta I = 0$) than for pure stretched dipole transitions ($\Delta I = 1$).

III. RESULTS

The ^{159}Er-level scheme constructed from the present paper is displayed in Figs. 1 and 2, whereas, a summary of the measurements obtained is presented in Table I.

A. The yrast band and Band 1

The lowest-energy band (labeled yrast in Figs. 1 and 2) was previously observed up to $I^\pi = (93/2^+)$ by Deleplanque *et al.* [24]. A parallel sequence was also observed at high-spin branching out from the $(85/2^+)$ yrast state. Both sequences were extended further to $(105/2^+)$ and $(101/2^+)$, respectively, by Kondev *et al.* [26], however, no explicit transition energies were published. In the present paper, excited states up to $(105/2^+)$ are observed, and new linking transitions have been established between states in the yrast band and the parallel sequence at high spins. Coincident γ-ray spectra, which show the high-energy part of the yrast band, are presented in Fig. 3. The photopeaks observed in Fig. 3(a) correspond to all of the transitions associated with the yrast band above the $53/2^+$ state; see the level scheme in Fig. 1. The γ-ray spectra of Figs. 3(b) and 3(c) were produced with a sum of triple gates in coincidence with individual transitions from the parallel sequence observed at this high energy and the yrast band, respectively. The multipolarity of the 1342-, 1264-, and 1292-keV linking transitions were measured and were found to be of stretched quadrupole character (see Table I), which establishes positive parity and positive signature $(\pi, \alpha) = (+, +1/2)$ for the connected levels.

Previously, the unfavored signature partner of the yrast structure with $(+, -1/2)$, initially established by Simpson *et al.* [22] and labeled band 1 in Fig. 1, was observed up to the $(43/2^+)$ state [24,26]. The present paper extends this band up to a possible $(91/2^+)$ with the observation of 14 new transitions associated with its decay. The spectrum of Fig. 4(a) was produced from a sum of triple gates and shows all of the transitions observed in band 1 above the $31/2^+$ excited state. This spectrum demonstrates the presence of the 1008- and 1269-keV parallel transitions at the highest spins in this band.

B. Bands 2 and 3

Previously, the band labeled band 2 in Fig. 1 was established up to the $(97/2^-)$ state by Deleplanque *et al.* [24]. Extensions were observed up to a further $(105/2^-)$ state [26], but no explicit transition energies were published. In the present paper, this sequence has been seen up to the $(105/2^-)$ state with the observation of the 1292- and 1188-keV transitions. The γ-ray spectra presented in Figs. 4(b) and 4(c) display the photopeaks that correspond to the γ decays of the states above $41/2^-$ in coincidence with the 1209- and 1292-keV transitions, respectively. Both spectra indicate the presence of the 1188-keV photopeak with no clear candidate for the decay of a higher-lying state.

Previously, the negative-parity band, band 3, had been observed from $(3/2^-)$ to $(15/2^-)$ and from $(27/2^-)$ to $(83/2^-)$ [24]. In the present paper, three new transitions have been observed, which connect the high- and low-spin parts of this band. In addition, the band has been extended up to $(91/2^-)$, and a parallel sequence, which originates from the $79/2^-$ state, is observed. In Fig. 5(a) a γ-ray spectrum is presented, which shows photopeaks that correspond to the transitions that connect the low- and high-spin structures of band 3. The

TABLE I. Excitation energies E_x, transition energies E_γ, intensities I_γ, angular intensity ratios R, and spin-parity assignments for the transitions observed in ^{159}Er from the present paper. The γ-ray energies are estimated to be accurate to ± 0.3 keV for the strong transitions ($I_\gamma > 10$), which rise to ± 0.6 keV for the weaker transitions. The intensity measurements have been normalized to the 349.9-keV ($21/2^+ \rightarrow 17/2^+$) yrast transition with a value of 100. The bands are labeled in order of the scheme shown in Figs. 1 and 2 and excitation energy E_x.

Band	E_x (keV)	E_γ (keV)	I_γ	R	Multipolarity	I^π_{initial}	I^π_{final}
Yrast							
	435.7	208.5	>100	0.71(1)	$E2$	$17/2^+$	$13/2^+$
	785.6	349.9	100	0.86(3)	$E2$	$21/2^+$	$17/2^+$
	1250.4	464.8	97.6(3.5)	0.84(3)	$E2$	$25/2^+$	$21/2^+$
	1806.5	556.1	71.5(2.2)	0.88(4)	$E2$	$29/2^+$	$25/2^+$
	2432.6	626.1	63.6(1.9)	0.98(3)	$E2$	$33/2^+$	$29/2^+$
	3108.5	675.9	44.0(1.3)	0.91(3)	$E2$	$37/2^+$	$33/2^+$
	3817.4	708.9	33.5(1.0)	0.95(4)	$E2$	$41/2^+$	$37/2^+$
	4556.0	738.7	25.6(8)	0.88(3)	$E2$	$45/2^+$	$41/2^+$
	5336.2	780.2	18.7(6)	0.99(4)	$E2$	$49/2^+$	$45/2^+$
	6166.7	830.4	13.7(4)	0.90(4)	$E2$	$53/2^+$	$49/2^+$
	7041.9	875.2	10.7(3)	0.92(4)	$E2$	$57/2^+$	$53/2^+$
	7946.5	904.5	7.2(2)	0.99(4)	$E2$	$61/2^+$	$57/2^+$
	8871.5	925.0	5.3(2)	1.01(5)	$E2$	$65/2^+$	$61/2^+$
	9826.2	954.7	4.2(1)	1.11(6)	$E2$	$69/2^+$	$65/2^+$
	10 822.5	996.3	3.0(1)	0.94(6)	$E2$	$73/2^+$	$69/2^+$
	11 866.8	1044.3	2.3(1)	0.88(5)	$E2$	$77/2^+$	$73/2^+$
	12 963.3	1096.4	1.7(1)	0.98(6)	$E2$	$81/2^+$	$77/2^+$
	14 116.7	1153.4	1.41(4)	1.04(8)	$E2$	$85/2^+$	$81/2^+$
	15 348.6	1231.9	0.75(2)	1.01(7)	$E2$	$89/2^+$	$85/2^+$
	15 458.8	1342.2	0.17(2)	1.06(21)	$E2$	$89/2^+$	$85/2^+$
	16 624.1	1275.7	0.41(2)	1.14(12)	$E2$	$93/2^+$	$89/2^+$
	16 612.6	1154.0	0.22(7)	1.04(18)	$E2$	$93/2^+$	$89/2^+$
		1263.3	0.17(2)	0.91(18)	$E2$	$93/2^+$	$89/2^+$
	17 677.4	1053.7	0.21(3)			$(97/2^+)$	$93/2^+$
		1064.4	0.12(3)			$(97/2^+)$	$93/2^+$
	17 916.4	1292.0	0.12(3)	1.09(24)	$E2$	$97/2^+$	$93/2^+$
		1304.0	0.08(2)	1.12(12)	$E2$	$97/2^+$	$93/2^+$
	18 618.6	941.2	0.14(3)			$(101/2^+)$	$(97/2^+)$
	(19 193)	(1277)				$(101/2^+)$	$97/2^+$
	(20 520)	(1327)				$(105/2^+)$	$(101/2^+)$
Band 1							
$1 \rightarrow$ Yrast	363.7	136.4	0.33(2)	0.46(4)	$M1/E2$	$11/2^+$	$13/2^+$
	591.3	227.4	0.60(2)	0.81(5)	$E2$	$15/2^+$	$11/2^+$
$1 \rightarrow$ Yrast		364.4	1.52(4)	0.62(4)	$M1/E2$	$15/2^+$	$13/2^+$
$1 \rightarrow$ Yrast		155.6	1.04(4)	0.62(4)	$M1/E2$	$15/2^+$	$17/2^+$
	961.7	370.6	6.0(1)	0.82(4)	$E2$	$19/2^+$	$15/2^+$
$1 \rightarrow$ Yrast		525.8	2.67(8)	0.63(5)	$M1/E2$	$19/2^+$	$17/2^+$
$1 \rightarrow$ Yrast		176.2	0.83(3)	0.48(4)	$M1/E2$	$19/2^+$	$21/2^+$
	1447.5	485.8	12.2(3)	0.84(3)	$E2$	$23/2^+$	$19/2^+$
$1 \rightarrow$ Yrast		661.7	1.87(5)	0.69(3)	$M1/E2$	$23/2^+$	$21/2^+$
$1 \rightarrow$ Yrast		197.2	1.04(3)	0.41(3)	$M1/E2$	$23/2^+$	$25/2^+$
	2025.8	578.3	15.2(3)	0.98(2)	$E2$	$27/2^+$	$23/2^+$
	2675.7	649.8	4.6(1)	0.93(3)	$E2$	$31/2^+$	$27/2^+$
$1 \rightarrow$ Yrast		869.0	0.17(1)			$31/2^+$	$29/2^+$
	3380.1	704.3	3.8(1)	1.00(5)	$E2$	$35/2^+$	$31/2^+$
	4127.8	747.7	3.23(5)	1.01(5)	$E2$	$39/2^+$	$35/2^+$
	4902.6	774.8	1.98(3)	0.93(4)	$E2$	$43/2^+$	$39/2^+$
	5656.6	754.0	0.78(3)	0.85(11)	$E2$	$47/2^+$	$43/2^+$
$1 \rightarrow$ Yrast		1101.5				$47/2^+$	$45/2^+$
	6448.7	792.1	0.65(3)	0.91(5)	$E2$	$51/2^+$	$47/2^+$
	7295.0	846.3	0.42(3)	0.82(3)	$E2$	$55/2^+$	$51/2^+$
	8166.2	871.2		0.92(7)	$E2$	$59/2^+$	$55/2^+$
	9037.3	871.0		0.92(7)	$E2$	$63/2^+$	$59/2^+$

TABLE I. (*Continued.*)

Band	E_x (keV)	E_γ (keV)	I_γ	R	Multipolarity	I^π_{initial}	I^π_{final}
	9925.6	888.3	0.16(2)			$(67/2^+)$	$63/2^+$
	10 847.1	921.5	0.09(2)	0.93(20)	$E2$	$(71/2^+)$	$(67/2^+)$
	11 815.8	968.7	0.07(2)	0.83(6)	$E2$	$(75/2^+)$	$(71/2^+)$
	12 849.6	1033.8	0.06(1)	0.96(7)	$E2$	$(79/2^+)$	$(75/2^+)$
	13 954.5	1105.0	0.04(1)			$(83/2^+)$	$(79/2^+)$
	15 116.4	1161.9	0.03(1)			$(87/2^+)$	$(83/2^+)$
	16 124.8	1008.5	0.01(1)			$(91/2^+)$	$(87/2^+)$
	16 385.4	1269.0	0.01(1)			$(91/2^+)$	$(87/2^+)$
Band 2							
	259.0	198.8	0.8(1)		$E2$[a,b]	$9/2^-$	$5/2^-$
$2 \rightarrow 3$		114.0	0.19(2)	0.45(5)	$M1/E2$	$9/2^-$	$7/2^-$
	574.0	315.1	2.33(4)	0.91(3)	$E2$	$13/2^-$	$9/2^-$
$2 \rightarrow 3$		143.6	0.79(1)	0.61(10)	$(M1/E2)$	$13/2^-$	$11/2^-$
	989.3	415.3	4.19(4)	0.82(3)	$E2$	$17/2^-$	$13/2^-$
$2 \rightarrow 3$		156.4	0.31(1)	0.44(9)	$M1/E2$	$17/2^-$	$15/2^-$
	1478.3	489.0	6.13(4)	0.83(3)	$E2$	$21/2^-$	$17/2^-$
	2011.0	532.8	9.45(6)	0.87(3)	$E2$	$25/2^-$	$21/2^-$
	2473.2	462.4	4.09(2)	0.83(2)	$E2$	$29/2^-$	$25/2^-$
$2 \rightarrow 1$		448.0	7.51(4)	0.43(3)	$E1$	$29/2^-$	$27/2^+$
$2 \rightarrow$ Yrast		666.6	2.00(3)	0.90(20)	$(E1)$	$29/2^-$	$29/2^+$
$2 \rightarrow 4$		386.0	4.54(3)	0.93(4)	$E2$	$29/2^-$	$25/2^-$
	2909.4	436.2	15.2(3)	0.87(3)	$E2$	$33/2^-$	$29/2^-$
	3436.1	526.7	14.7(3)	0.96(3)	$E2$	$37/2^-$	$33/2^-$
	4061.6	625.5	14.1(3)	0.98(3)	$E2$	$41/2^-$	$37/2^-$
	4782.4	720.8	12.2(2)	0.97(3)	$E2$	$45/2^-$	$41/2^-$
	5583.2	800.8	9.7(2)	0.95(4)	$E2$	$49/2^-$	$45/2^-$
	6434.2	851.0	6.9(2)	0.96(4)	$E2$	$53/2^-$	$49/2^-$
	7292.1	857.8	4.92(9)	1.00(5)	$E2$	$57/2^-$	$53/2^-$
	8158.7	866.7	3.30(6)	1.01(6)	$E2$	$61/2^-$	$57/2^-$
	9070.8	912.1	2.49(6)	0.93(3)	$E2$	$65/2^-$	$61/2^-$
	10 045.3	974.4	1.74(4)	0.93(4)	$E2$	$69/2^-$	$65/2^-$
	11 089.6	1044.4	1.28(3)	0.93(4)	$E2$	$73/2^-$	$69/2^-$
	12 199.4	1109.8				$(77/2^-)$	$73/2^-$
	13 326.1	1126.7	0.65(2)	0.89(9)	$E2$	$(81/2^-)$	$(77/2^-)$
	14 435.6	1109.8				$(85/2^-)$	$(81/2^-)$
	15 538.7	1103.1	0.31(2)	0.98(20)	$E2$	$(89/2^-)$	$(85/2^-)$
	16 683.5	1144.9	0.19(2)	0.93(9)	$E2$	$(93/2^-)$	$(89/2^-)$
	17 892.2	1208.6	0.14(1)	0.97(17)	$E2$	$(97/2^-)$	$(93/2^-)$
	19 184.0	1291.9	0.06(1)			$(101/2^-)$	$(97/2^-)$
	20 372.1	1188.1	0.02(1)			$(105/2^-)$	$(101/2^-)$
Band 3							
	145.2	145.2	0.52(7)	0.80(4)	$E2$	$7/2^-$	$3/2^-$
	429.8	284.5	0.57(2)	0.82(5)	$E2$	$11/2^-$	$7/2^-$
$3 \rightarrow 2$		170.3	0.19(2)	0.40(7)	$M1/E2$	$11/2^-$	$9/2^-$
	833.0	403.2	0.15(2)		$E2$[b]	$15/2^-$	$11/2^-$
$3 \rightarrow 2$		260.2	0.11(2)			$15/2^-$	$13/2^-$
	1323.6	490.0	0.05(1)			$(19/2^-)$	$15/2^-$
	1849.2	524.7	0.03(2)			$(23/2^-)$	$(19/2^-)$
	2259.8	410.4	0.03(2)			$27/2^-$	$(23/2^-)$
$3 \rightarrow$ Yrast		1009.4	1.38(6)	0.53(7)	$E1$	$27/2^-$	$25/2^+$
	2661.6	401.9	1.8(1)	1.00(7)	$E2$	$31/2^-$	$27/2^-$
$3 \rightarrow$ Yrast		855.4	7.1(2)	0.65(3)	$E1$	$31/2^-$	$29/2^+$
	3146.2	484.9	7.5(2)	0.97(5)	$E2$	$35/2^-$	$31/2^-$
$3 \rightarrow$ Yrast		713.5	5.6(2)	0.44(6)	$E1$	$35/2^-$	$33/2^+$
	3733.9	587.8	10.2(2)	0.93(7)	$E2$	$39/2^-$	$35/2^-$
	4421.2	687.3	7.3(2)	0.92(4)	$E2$	$43/2^-$	$39/2^-$
	5193.5	772.3	7.2(2)	0.98(4)	$E2$	$47/2^-$	$43/2^-$

TABLE I. (*Continued*.)

Band	E_x (keV)	E_γ (keV)	I_γ	R	Multipolarity	I^π_{initial}	I^π_{final}
	6026.9	833.3	5.6(1)	0.93(7)	$E2$	$51/2^-$	$47/2^-$
	6883.5	856.6	3.7(1)		$E2$[b]	$55/2^-$	$51/2^-$
	7753.9	870.4	2.7(1)	0.97(5)	$E2$	$59/2^-$	$55/2^-$
	8665.4	911.4	1.74(5)	0.98(5)	$E2$	$63/2^-$	$59/2^-$
	9633.7	968.3	1.18(3)	1.01(6)	$E2$	$67/2^-$	$63/2^-$
	10 661.4	1027.7	0.82(2)	0.91(9)	$E2$	$71/2^-$	$67/2^-$
	11 748.0	1086.7	0.55(2)	0.91(9)	$E2$	$75/2^-$	$71/2^-$
	12 895.1	1147.1	0.44(2)	0.92(10)	$E2$	$79/2^-$	$75/2^-$
	14 104.0	1208.9	0.22(2)	0.97(11)	$E2$	$83/2^-$	$79/2^-$
	14 117.3	1222.2	0.08(2)			$(83/2^-)$	$79/2^-$
	15 336.3	1232.4	0.07(2)			$(87/2^-)$	$83/2^-$
	15 342.5	1225.1	0.03(1)			$(87/2^-)$	$(83/2^-)$
	(16 633)	(1297)				$(91/2^-)$	$(87/2^-)$
Band 4							
$4 \rightarrow 1$	2087.2	640.1	4.90(9)	0.65(2)	$E1$	$25/2^-$	$23/2^+$
	2550.8	463.8	0.76(5)	0.81(20)	$E2$	$29/2^-$	$25/2^-$
$4 \rightarrow 2$		539.7	4.6(1)	0.99(4)	$E2$	$29/2^-$	$25/2^-$
$4 \rightarrow$ Yrast		745.1	0.59(3)			$29/2^-$	$29/2^+$
	3097.8	546.9	3.7(1)	0.94(5)	$E2$	$33/2^-$	$29/2^-$
$4 \rightarrow 2$		625.4	1.1(1)	0.78(3)	$E2$	$33/2^-$	$29/2^-$
	3694.1	596.3	4.11(6)	0.85(7)	$E2$	$37/2^-$	$33/2^-$
	4351.7	657.7	3.51(5)	0.97(4)	$E2$	$41/2^-$	$37/2^-$
	5073.4	721.6	2.78(6)	0.91(3)	$E2$	$45/2^-$	$41/2^-$
	5849.8	776.4	2.16(4)	1.14(6)	$E2$	$49/2^-$	$45/2^-$
	6669.1	819.3	1.66(4)	0.96(6)	$E2$	$53/2^-$	$49/2^-$
	7534.8	865.7	1.28(3)	0.92(7)	$E2$	$57/2^-$	$53/2^-$
	8440.6	905.8	0.83(3)	0.98(7)	$E2$	$61/2^-$	$57/2^-$
	9358.4	917.8	0.58(3)	0.89(7)	$E2$	$65/2^-$	$61/2^-$
	10 307.6	949.2	0.45(2)	1.02(8)	$E2$	$69/2^-$	$65/2^-$
	11 302.6	995.1	0.39(2)	0.97(8)	$E2$	$73/2^-$	$69/2^-$
	12 348.9	1046.2	0.25(2)	0.98(21)	$E2$	$77/2^-$	$73/2^-$
	13 421.6	1072.7	0.09(2)			$(81/2^-)$	$77/2^-$
	(13 460)	(1111)				$(81/2^-)$	$77/2^-$
	(14 561)	(1140)				$(85/2^-)$	$(81/2^-)$
Band 5							
$5 \rightarrow 2$	2665.0	654.0	1.26(3)	0.96(6)	$E2$	$29/2^-$	$25/2^-$
	3235.1	570.0	1.43(2)	0.91(3)	$E2$	$33/2^-$	$29/2^-$
	3852.2	617.1	1.28(3)	0.84(3)	$E2$	$37/2^-$	$33/2^-$
	4515.5	663.4	0.91(2)	0.97(6)	$E2$	$41/2^-$	$37/2^-$
	5235.2	719.7	0.84(3)	0.96(6)	$E2$	$45/2^-$	$41/2^-$
	6006.4	771.2	0.67(2)	0.93(9)	$E2$	$49/2^-$	$45/2^-$
	6802.6	796.2	0.36(2)	0.92(8)	$E2$	$53/2^-$	$49/2^-$
	7636.2	833.6	0.21(2)	1.00(10)	$E2$	$57/2^-$	$53/2^-$
	8530.6	894.4	0.15(2)	0.76(9)	$E2$	$61/2^-$	$57/2^-$
	9483.7	953.1	0.07(3)			$(65/2^-)$	$61/2^-$
	10 464.8	981.2	0.04(2)			$(69/2^-)$	$(65/2^-)$
	(11 499)	(1035)				$(73/2^-)$	$(69/2^-)$
γ band							
$\gamma \rightarrow 1$	1090.8	(499)				$(17/2^+)$	$15/2^+$
	1451.0	360.2	0.27(5)			$21/2^+$	$(17/2^+)$
$\gamma \rightarrow$ Yrast		1015.0	0.40(4)	0.86(10)	$E2$	$21/2^+$	$17/2^+$
$\gamma \rightarrow$ Yrast		666.0	0.09(2)			$21/2^+$	$21/2^+$
$\gamma \rightarrow 1$		490.2	0.08(2)			$21/2^+$	$19/2^+$
	1889.9	438.1	0.85(4)	1.12(13)	$E2$	$25/2^+$	$21/2^+$
$\gamma \rightarrow$ Yrast		1104.3	0.80(8)			$25/2^+$	$21/2^+$
$\gamma \rightarrow$ Yrast		(639)				$25/2^+$	$25/2^+$
	2386.0	496.7	1.26(3)	1.06(9)	$E2$	$29/2^+$	$25/2^+$

TABLE I. (*Continued.*)

Band	E_x (keV)	E_γ (keV)	I_γ	R	Multipolarity	I^π_{initial}	I^π_{final}
$\gamma \rightarrow$ Yrast		1135.0	0.97(6)	1.10(14)	$E2$	$29/2^+$	$21/2^+$
	2935.1	548.8	1.29(2)	0.98(13)	$E2$	$33/2^+$	$29/2^+$
$\gamma \rightarrow$ Yrast		1128.2	0.67(4)	0.81(9)	$E2$	$33/2^+$	$29/2^+$
	3544.9	609.6	1.84(5)	0.91(9)	$E2$	$37/2^+$	$33/2^+$
$\gamma \rightarrow$ Yrast		1112.3	0.86(5)	0.86(8)	$E2$	$37/2^+$	$33/2^+$
	4226.5	681.4	1.42(4)	0.98(15)	$E2$	$41/2^+$	$37/2^+$
$\gamma \rightarrow$ Yrast		1118.8	0.58(4)	0.86(12)	$E2$	$41/2^+$	$37/2^+$
	4984.5	758.0	1.55(5)	0.85(12)	$E2$	$45/2^+$	$41/2^+$
$\gamma \rightarrow$ Yrast		1167.3	0.73(2)	0.97(10)	$E2$	$45/2^+$	$41/2^+$
	5790.5	806.0	1.28(4)	0.86(13)	$E2$	$49/2^+$	$45/2^+$
$\gamma \rightarrow$ Yrast		1233.1	0.33(4)	1.16(16)	$E2$	$45/2^+$	$41/2^+$
	6612.6	822.0	0.78(4)	0.97(10)	$E2$	$53/2^+$	$49/2^+$
	7473.0	860.5	0.54(3)	0.99(13)	$E2$	$57/2^+$	$53/2^+$
	8397.9	923.3	0.43(3)	0.87(22)	$E2$	$61/2^+$	$57/2^+$
$\gamma \rightarrow$ Yrast		1357.3	0.03(1)			$61/2^+$	$57/2^+$
	9386.3	988.4	0.23(2)			$(65/2^+)$	$61/2^+$
	10 397.1	1010.8	0.11(2)			$(69/2^+)$	$(65/2^+)$
	11 392.8	995.7	0.08(2)			$(73/2^+)$	$(69/2^+)$
	12 434.8	1041.9	0.07(2)			$(77/2^+)$	$(73/2^+)$
Band 6							
$6 \rightarrow$ Yrast	2230.0	1794.2	0.06(2)			$(19/2^-)$	$17/2^+$
$6 \rightarrow$ Yrast		1444.4	0.02(1)			$(19/2^-)$	$21/2^+$
$6 \rightarrow 7$	2389.5	99.0	0.06(2)			$23/2^-$	$(21/2^-)$
	2681.6	292.1			$E2^{rmb}$	$27/2^-$	$23/2^-$
$6 \rightarrow 7$		162.0	1.66(5)	0.55(20)	$M1/E2$	$27/2^-$	$25/2^-$
	3097.2	415.4	0.62(3)	0.88(10)	$E2$	$31/2^-$	$27/2^-$
$6 \rightarrow 7$		222.4	1.66(5)	0.57(10)	$M1/E2$	$31/2^-$	$29/2^-$
	3618.5	521.7	2.05(6)	0.94(6)	$E2$	$35/2^-$	$31/2^-$
$6 \rightarrow 7$		272.5	2.99(9)	0.58(2)	$M1/E2$	$35/2^-$	$33/2^-$
	4224.0	605.8	2.35(9)	0.91(10)	$E2$	$39/2^-$	$35/2^-$
$6 \rightarrow 7$		312.1	2.40(7)	0.57(2)	$M1/E2$	$39/2^-$	$37/2^-$
	4891.1	667.7	2.09(6)	0.91(4)	$E2$	$43/2^-$	$39/2^-$
$6 \rightarrow 7$		340.4	1.87(6)	0.62(3)	$M1/E2$	$43/2^-$	$41/2^-$
	5599.5	707.9	1.92(6)	0.94(4)	$E2$	$47/2^-$	$43/2^-$
$6 \rightarrow 7$		357.6	1.42(4)	0.44(6)	$M1/E2$	$47/2^-$	$45/2^-$
	6332.4	733.3	1.47(4)	0.95(5)	$E2$	$51/2^-$	$47/2^-$
$6 \rightarrow 7$		369.8	1.43(4)	0.59(6)	$M1/E2$	$51/2^-$	$49/2^-$
	7097.7	765.4	1.19(4)	0.89(6)	$E2$	$55/2^-$	$51/2^-$
$6 \rightarrow 7$		387.5	1.21(4)	0.64(8)	$M1/E2$	$55/2^-$	$53/2^-$
	7912.5	814.7	0.96(3)	1.08(8)	$E2$	$59/2^-$	$55/2^-$
$6 \rightarrow 7$		414.3	0.72(3)	0.64(7)	$M1/E2$	$59/2^-$	$57/2^-$
	8789.0	876.9	0.81(3)	0.96(7)	$E2$	$63/2^-$	$59/2^-$
$6 \rightarrow 7$		445.3	0.67(3)	0.65(8)	$M1/E2$	$63/2^-$	$61/2^-$
	9732.7	943.4	0.63(2)	0.86(5)	$E2$	$67/2^-$	$63/2^-$
$6 \rightarrow 7$		479.5	0.34(2)	0.47(6)	$M1/E2$	$67/2^-$	$65/2^-$
	10 742.7	1010.6	0.48(2)	0.92(8)	$E2$	$71/2^-$	$67/2^-$
$6 \rightarrow 7$		510.3	0.24(2)	0.55(8)	$M1/E2$	$71/2^-$	$69/2^-$
	11 815.4	1072.4	0.41(4)	0.91(11)	$E2$	$75/2^-$	$71/2^-$
$6 \rightarrow 7$		540.8	0.17(2)		$(M1/E2)$	$75/2^-$	$73/2^-$
	12 940.1	1124.8	0.32(2)	0.90(12)	$E2$	$79/2^-$	$75/2^-$
	14 136.6	1196.5	0.07(2)			$(83/2^-)$	$79/2^-$
	(15 340)	(1203)				$(87/2^-)$	$(83/2^-)$
	(16 558)	(1218)				$(91/2^-)$	$(87/2^-)$
Band 7							
$7 \rightarrow$ Yrast	1713.5	928.6	0.27(5)	0.56(12)	$E1$ or $M1$	$23/2^{(+)}$	$21/2^+$
$7 \rightarrow 6$	2290.3	59				$(21/2^-)$	$(19/2^-)$
$7 \rightarrow 6$	2519.5	130.4	0.17(1)	0.48(6)	$M1/E2$	$25/2^-$	$23/2^-$

TABLE I. (*Continued*.)

Band	E_x (keV)	E_γ (keV)	I_γ	R	Multipolarity	I^π_{initial}	I^π_{final}
7 → Yrast		1270.6	1.09(3)	0.80(14)	$E1$	$25/2^-$	$25/2^+$
7 → 1		1072.2	0.17(2)		$E1$[b]	$25/2^-$	$23/2^+$
7 → 2		1041.4	0.38(2)		$E2$[b]	$25/2^-$	$21/2^-$
		806.8	0.38(2)	0.45(7)	$E1$ or $M1$	$25/2^-$	$23/2^{(+)}$
	2874.8	356.9			$E2$[b]	$29/2^-$	$25/2^-$
7 → 6		193.4	2.12(3)	0.65(4)	$M1/E2$	$29/2^-$	$27/2^-$
	3345.8	471.4	0.97(2)	0.92(5)	$E2$	$33/2^-$	$29/2^-$
7 → 6		248.5	3.3(1)	0.58(4)	$M1/E2$	$33/2^-$	$31/2^-$
	3911.8	566.1	1.97(6)	0.85(6)	$E2$	$37/2^-$	$33/2^-$
7 → 6		293.0	2.97(9)	0.60(4)	$M1/E2$	$37/2^-$	$35/2^-$
	4550.7	639.4	2.06(6)	0.90(4)	$E2$	$41/2^-$	$37/2^-$
7 → 6		326.6	2.00(6)	0.61(4)	$M1/E2$	$41/2^-$	$39/2^-$
	5242.0	690.7	1.99(6)	1.00(6)	$E2$	$45/2^-$	$41/2^-$
7 → 6		350.9	1.44(5)	0.61(6)	$M1/E2$	$45/2^-$	$43/2^-$
	5962.6	721.0	1.55(4)	0.95(4)	$E2$	$49/2^-$	$45/2^-$
7 → 6		363.1	1.50(5)	0.62(6)	$M1/E2$	$49/2^-$	$47/2^-$
	6710.0	747.7	1.25(4)	0.93(6)	$E2$	$53/2^-$	$49/2^-$
7 → 6		377.3	1.23(4)	0.58(4)	$M1/E2$	$53/2^-$	$51/2^-$
	7498.3	788.4	1.03(3)	0.84(6)	$E2$	$57/2^-$	$53/2^-$
7 → 6		400.6	0.90(3)	0.55(4)	$M1/E2$	$57/2^-$	$55/2^-$
	8343.4	845.0	0.98(3)	0.88(6)	$E2$	$61/2^-$	$57/2^-$
7 → 6		430.7	0.69(3)	0.62(8)	$M1/E2$	$61/2^-$	$59/2^-$
	9253.4	910.0	0.74(2)	0.95(9)	$E2$	$65/2^-$	$61/2^-$
7→6		464.6				$65/2^-$	$63/2^-$
	10 231.2	977.9	0.60(2)	0.91(11)	$E2$	$69/2^-$	$65/2^-$
7 → 6		497.7	0.40(2)	0.64(10)	$M1/E2$	$69/2^-$	$67/2^-$
	11 274.7	1044.3	0.31(3)	0.86(12)	$E2$	$73/2^-$	$69/2^-$
7 → 6		531.4	0.21(2)			$73/2^-$	$71/2^-$
	12 384.2	1109.5	0.22(2)	0.87(13)	$E2$	$77/2^-$	$73/2^-$
	13 528.5	1144.3	0.07(2)			$(81/2^-)$	$77/2^-$
	13 550.5	1166.3	0.06(2)			$(81/2^-)$	$77/2^-$
	14 737.1	1208.6	0.06(2)			$(85/2^-)$	$(81/2^-)$
	14 754.7	1204.2	0.05(2)			$(85/2^-)$	$(81/2^-)$
	(16 107)	(1352)				$(89/2^-)$	$(85/2^-)$
Band 8							
8 → 9	3987.5	241.0	0.05(1)	0.64(30)	$(M1/E2)$	$(33/2^+)$	$(31/2^+)$
	4450.9	463.0	0.09(1)			$(37/2^+)$	$(33/2^+)$
8 → 9		203.0	0.10(1)	0.57(14)	$M1/E2$	$(37/2^+)$	$(35/2^+)$
8 → 6		832.6	0.22(2)	0.46(7)	$E1$ or $M1$	$37/2^{(+)}$	$35/2^-$
	4891.9	441.4	0.27(6)	0.81(21)	$E2$	$(41/2^+)$	$(37/2^+)$
8 → 9		225.8	0.49(1)	0.48(4)	$M1/E2$	$(41/2^+)$	$(39/2^+)$
	5402.7	511.1	0.65(2)			$(45/2^+)$	$(41/2^+)$
8 → 9		265.6	0.93(2)	0.64(4)	$M1/E2$	$(45/2^+)$	$(43/2^+)$
	6014.3	611.6	0.53(2)	0.83(6)	$E2$	$(49/2^+)$	$(45/2^+)$
8 → 9		318.3	0.89(3)	0.62(6)	$M1/E2$	$(49/2^+)$	$(47/2^+)$
	6724.8	710.4	0.54(2)	1.02(6)	$E2$	$(53/2^+)$	$(49/2^+)$
8 → 9		367.4	0.74(2)	0.43(6)	$M1/E2$	$(53/2^+)$	$(51/2^+)$
	7530.0	805.5	0.47(2)	1.03(10)	$E2$	$(57/2^+)$	$(53/2^+)$
8 → 9		414.3	0.46(2)	0.58(6)	$M1/E2$	$(57/2^+)$	$(55/2^+)$
	8421.2	890.9	0.39(2)	0.84(7)	$E2$	$(61/2^+)$	$(57/2^+)$
8 → 9		455.8	0.38(2)			$(61/2^+)$	$(59/2^+)$
	9385.8	964.3	0.21(1)	0.98(19)	$E2$	$(65/2^+)$	$(61/2^+)$
8 → 9		490.8	0.11(1)			$(65/2^+)$	$(63/2^+)$
	10 391.2	1005.4	0.09(1)			$(69/2^+)$	$(65/2^+)$
	11 405.8	1014.6	0.06(1)			$(73/2^+)$	$(69/2^+)$
Band 9							
	4248.1	501.0	0.03(1)			$(35/2^+)$	$(31/2^+)$

TABLE I. (*Continued.*)

Band	E_x (keV)	E_γ (keV)	I_γ	R	Multipolarity	I^π_{initial}	I^π_{final}
$9 \rightarrow 8$		261.3	0.07(1)			$(35/2^+)$	$(33/2^+)$
	4666.0	418.0	0.17(1)			$(39/2^+)$	$(35/2^+)$
$9 \rightarrow 8$		215.0	0.31(2)	0.59(10)	$M1/E2$	$(39/2^+)$	$(37/2^+)$
$9 \rightarrow 7$		(754)				$(39/2^+)$	$37/2^-$
	5136.9	470.7	0.54(5)	0.86(12)	$E2$	$(43/2^+)$	$(39/2^+)$
$9 \rightarrow 8$		245.0	0.72(2)	0.45(13)	$M1/E2$	$(43/2^+)$	$(41/2^+)$
	5696.0	558.9	0.76(1)	0.85(12)	$E2$	$(47/2^+)$	$(43/2^+)$
$9 \rightarrow 8$		293.3	1.07(2)	0.57(12)	$M1/E2$	$(47/2^+)$	$(45/2^+)$
	6357.2	661.5	0.67(1)	0.90(12)	$E2$	$(51/2^+)$	$(47/2^+)$
$9 \rightarrow 8$		342.9	0.81(3)	0.65(12)	$M1/E2$	$(51/2^+)$	$(49/2^+)$
	7115.6	758.7	0.54(2)	0.87(10)	$E2$	$(55/2^+)$	$(51/2^+)$
$9 \rightarrow 8$		390.8	0.64(2)	0.48(15)	$M1/E2$	$(55/2^+)$	$(53/2^+)$
	7965.5	849.7	0.55(2)	0.85(13)	$E2$	$(59/2^+)$	$(55/2^+)$
$9 \rightarrow 8$		435.6	0.43(2)			$(59/2^+)$	$(57/2^+)$
	8895.2	930.0	0.34(1)	0.85(13)	$E2$	$(63/2^+)$	$(59/2^+)$
$9 \rightarrow 8$		474.0	0.22(1)			$(63/2^+)$	$(61/2^+)$
	9878.9	983.8	0.31(1)	0.85(16)	$E2$	$(67/2^+)$	$(63/2^+)$
$9 \rightarrow 8$		492.9	0.08(1)			$(67/2^+)$	$(65/2^+)$
	10 871.2	992.3	0.11(1)			$(71/2^+)$	$(67/2^+)$
	11 893.9	1022.7	0.07(1)			$(75/2^+)$	$(71/2^+)$
	12 962.5	1068.6	0.06(1)			$(79/2^+)$	$(75/2^+)$
Band 10							
$10 \rightarrow$ Yrast	6364.7	1027.6	0.10(2)			$(51/2^-)$	$49/2^+$
	7170.2	804.7	0.10(1)			$55/2^-$	$(51/2^-)$
$10 \rightarrow 3$		1143.3	0.13(1)	0.94(16)	$E2$	$55/2^-$	$51/2^-$
$10 \rightarrow$ Yrast		1004.9	0.13(1)			$55/2^-$	$53/2^+$
	8053.6	883.7	0.24(1)	0.99(10)	$E2$	$59/2^-$	$55/2^-$
$10 \rightarrow 3$		1169.7	0.04(1)			$59/2^-$	$55/2^-$
	8998.4	944.8	0.39(1)	0.93(7)	$E2$	$63/2^-$	$59/2^-$
	10 002.4	1004.0	0.38(1)	0.85(8)	$E2$	$67/2^-$	$63/2^-$
	11 043.4	1041.0	0.31(1)			$(71/2^-)$	$67/2^-$
	12 097.7	1054.3	0.30(1)			$(75/2^-)$	$(71/2^-)$
	13 183.0	1085.3	0.12(1)			$(79/2^-)$	$(75/2^-)$
	14 329.7	1146.7	0.07(1)			$(83/2^-)$	$(79/2^-)$
	15 540.8	1211.1	0.07(1)			$(87/2^-)$	$(83/2^-)$
	16 839.8	1299.0	0.04(1)			$(91/2^-)$	$(87/2^-)$
	(18 175)	(1335)				$(95/2^-)$	$(91/2^-)$

[a]Taken from Ref. [23].
[b]Taken from Ref. [24].

spectra of Figs. 6(a) and 6(b) provide the high-energy part of this band. They were produced with a sum of triple gates set on the transitions in band 3, in coincidence with gates at 1209 and 1222 keV, Figs. 6(a) and 6(b), respectively. Photopeaks are observed at 1232 and (1297) keV in coincidence with the 1209-keV transition and 1225 keV for the 1222-keV transition, which establishes a parallel sequence above the $79/2^-$ state. The spectra also indicate a dramatic drop in photopeak intensity above this state.

C. Bands 4, 5, and 10

Previously, band 4 was observed up to a possible $(77/2^-)$ state [24], and it has been extended by one transition in the present paper with two tentative transitions, which are observed at higher spins. A γ-ray spectrum of the high-energy part of this band is presented in Fig. 7(a).

Previously, band 5 was observed up to a $41/2^-$ state [24]. It was linked to band 2 via a connecting stretched $E2$ transition of energy 570 keV. In the present paper, a transition of energy 654 keV has been found to be the connecting transition that links these two bands with the 570-keV transition, which is part of band 5. In addition, band 5 has been extended by six transitions (and one tentative transition), which takes it up to a possible $(73/2^-)$ state. These new transitions can be seen in the γ-ray spectrum of Fig. 5(b) where the full band is presented. The multipolarity of the 654-keV linking transition was measured and was found to be of a stretched quadrupole character (see Table I), which confirms the previous assignment of negative parity for band 5.

In a previous paper by Deleplanque *et al.* [24], three tentative transitions, with energies of 1053, 1005, and 941 keV, were observed in coincidence. They were thought to be

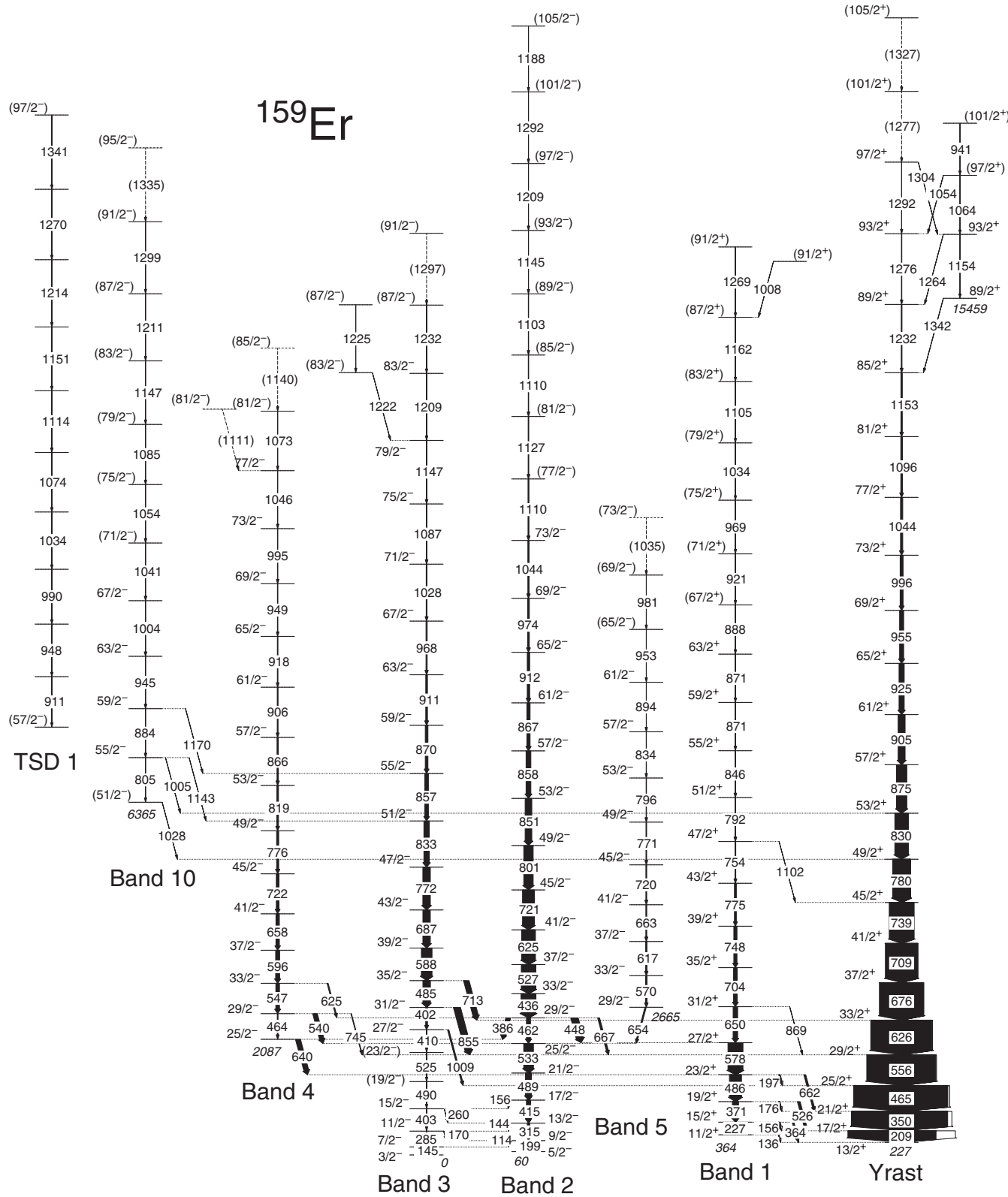

FIG. 1. Partial-level scheme for ^{159}Er constructed from the present paper; see Fig. 2 for the remainder of the scheme. Transition energies and the excitation energy of the band heads are given to the nearest keV. The width of the arrows represents the relative intensity of the transitions with the unshaded regions attributed to internal conversion. Spin assignments and excitation energy of the band labeled TSD 1 are based on comparisons with results from CNS calculations; see text as well as Ref. [20].

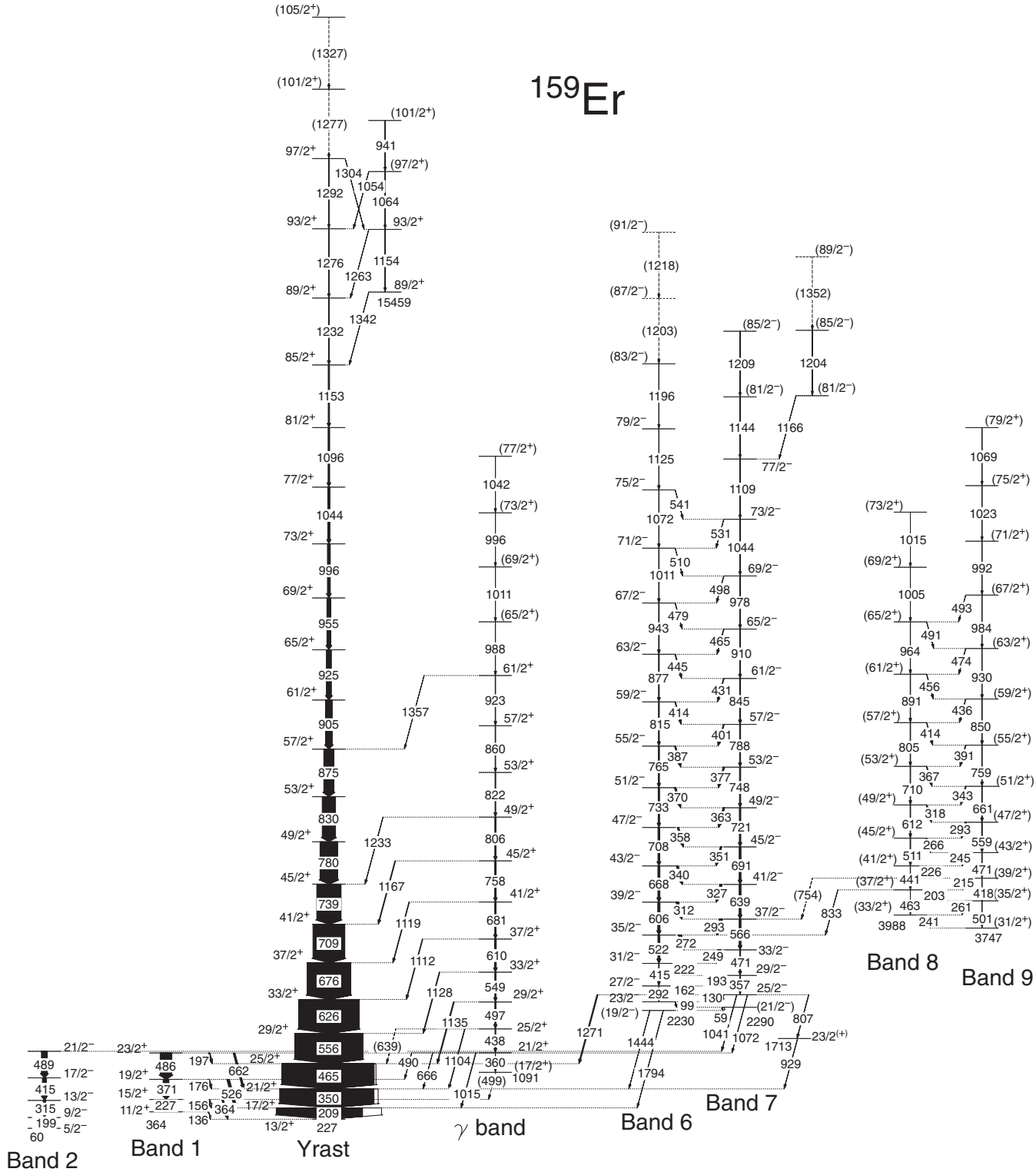

FIG. 2. Partial-level scheme for ^{159}Er constructed from the present paper for the strongly coupled bands; see Fig. 1 for the remainder of the scheme. Transition energies and the excitation energy of the band heads are given to the nearest keV. The width of the arrows represents the relative intensity of the transitions with the unshaded regions attributed to internal conversion.

linked to the main-level scheme through the $81/2^+$ yrast state. In the present paper, these transitions have been found to be part of a new rotational sequence, band 10, which extends from $(51/2^-)$ up to a probable $(95/2^-)$ state. Photopeaks associated with the transitions observed in this band are present in the γ-ray spectrum of Fig. 7(b). Four linking transitions have also

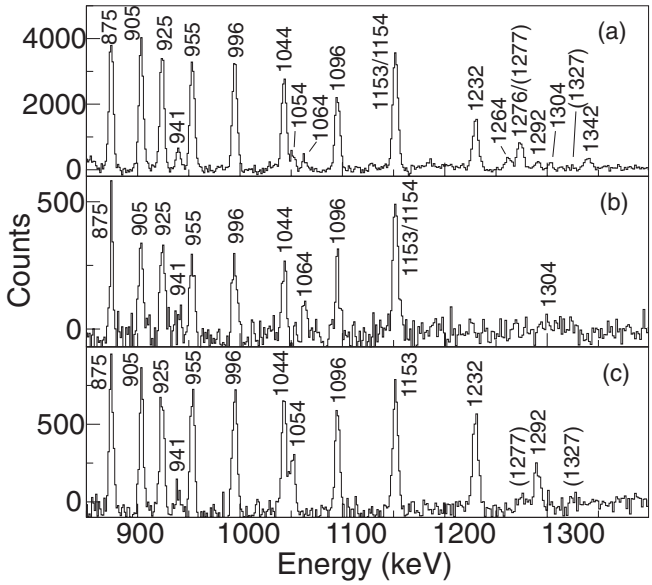

FIG. 3. Background-subtracted γ-ray spectra from the E_γ^4 hypercube produced with (a) a sum of triple gates set on the yrast band, (b) a sum of triple gates set on the 830–1153(1154)-keV transitions in coincidence with the 1342-keV transition, and (c) a sum of triple gates set on the 830–1232-keV transitions (excluding the 1153- to 1154-keV transitions) in coincidence with the 1276-keV transition.

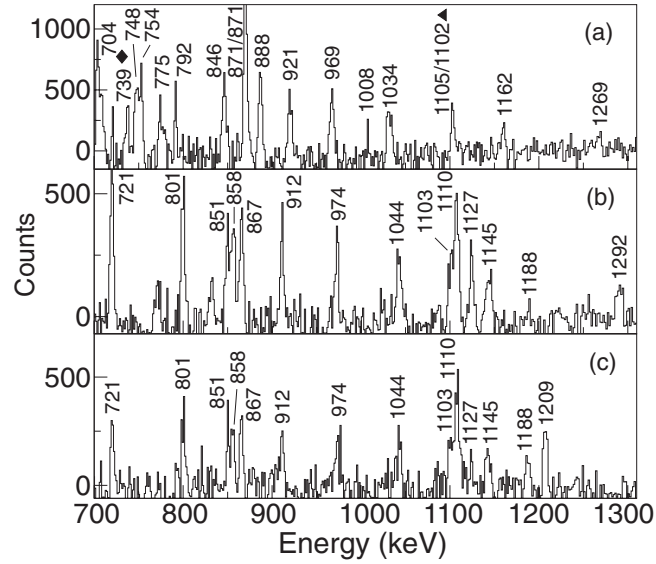

FIG. 4. Background-subtracted γ-ray spectra from the E_γ^4 hypercube produced with (a) a sum of triple gates set on band 1 above the $47/2^+$ state to the $(87/2^+)$ state and a sum of triple gates set on band 2 up to the $(93/2^-)$ state in coincidence with (b) the 1209-keV transition and (c) the 1292-keV transition. Photopeaks that correspond to linking transitions are labeled with triangles, and photopeaks within the yrast band are labeled with diamonds.

been observed, connecting this band to band 3 and the yrast band. From the angular-intensity ratio measurement (Table I), the multipolarity of the 1143-keV transition was extracted and was found to be of stretched quadrupole nature, which suggested negative parity for this band.

TABLE II. Quasiparticle labeling scheme for ^{159}Er based on the predominant Nilsson components at $\hbar\omega = 0$ MeV and their parity and signature (π, α). Note that the $\nu h_{9/2}$ and $f_{7/2}$ orbitals are highly mixed.

	Label	$(\pi, \alpha)_n$	Nilsson orbital at $\hbar\omega = 0$ MeV
Quasineutrons	A	$(+, +1/2)_1$	$i_{13/2}[651]3/2$
	B	$(+, -1/2)_1$	$i_{13/2}[651]3/2$
	C	$(+, +1/2)_2$	$i_{13/2}[660]1/2$
	D	$(+, -1/2)_2$	$i_{13/2}[660]1/2$
	E	$(-, +1/2)_1$	$f_{7/2}[521]3/2$
	F	$(-, -1/2)_1$	$f_{7/2}[521]3/2$
	G	$(-, +1/2)_2$	$h_{9/2}[523]5/2$
	H	$(-, -1/2)_2$	$h_{9/2}[523]5/2$
Quasiprotons	A_p	$(-, -1/2)_1$	$h_{11/2}[523]7/2$
	B_p	$(-, +1/2)_1$	$h_{11/2}[523]7/2$
	C_p	$(-, -1/2)_2$	$h_{9/2}[541]1/2$
	D_p	$(-, +1/2)_2$	$h_{9/2}[541]1/2$
	E_p	$(+, -1/2)_1$	$g_{7/2}[404]7/2$
	F_p	$(+, +1/2)_1$	$g_{7/2}[404]7/2$

D. The γ band

A new band, labeled the γ band in Fig. 2, has been observed in the current paper. It consists of 15 intraband transitions and is connected to the yrast band through a series of high-energy (>1 MeV) γ decays. The multipolarity of seven of these connecting transitions was measured and was found to be consistent with them and to be of stretched quadrupole character, which assigned this band to be of positive parity

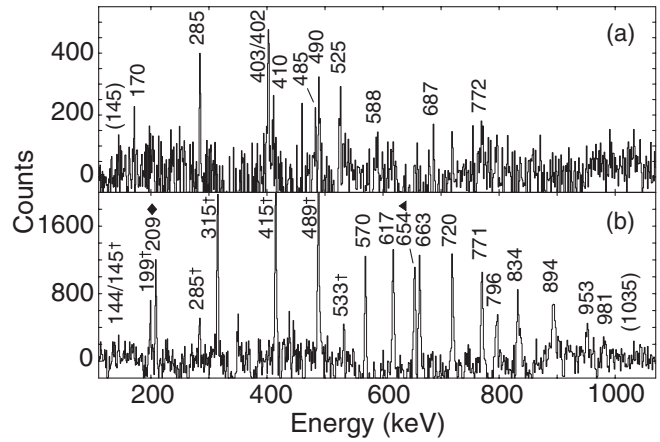

FIG. 5. Background-subtracted γ-ray spectra from the E_γ^4 hypercube produced with (a) a sum of triple gates set on transitions in band 3 to display the low- and high-spin parts of this sequence and (b) a sum of triple gates set on band 5. Photopeaks that correspond to linking transitions are labeled with triangles, photopeaks within the yrast band are labeled with diamonds, and photopeaks labeled with crosses correspond to transitions within band 2.

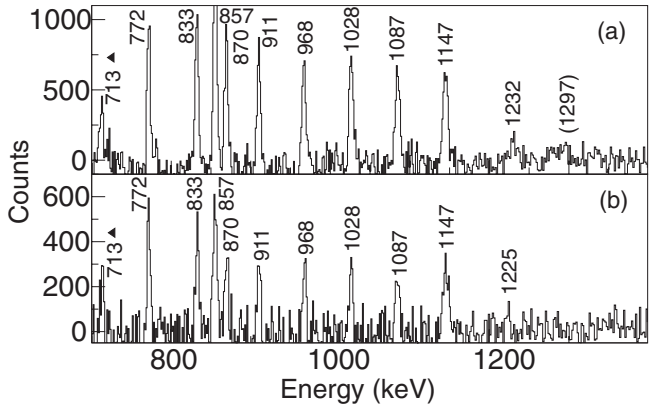

FIG. 6. Background-subtracted γ-ray spectra from the E_γ^4 hypercube produced with a sum of triple gates set on band 3 from the decay of the $39/2^-$ state to the $79/2^-$ state in coincidence with (a) the 1209-keV transitions and (b) the 1222-keV transition. Photopeaks that correspond to linking transitions are labeled with triangles.

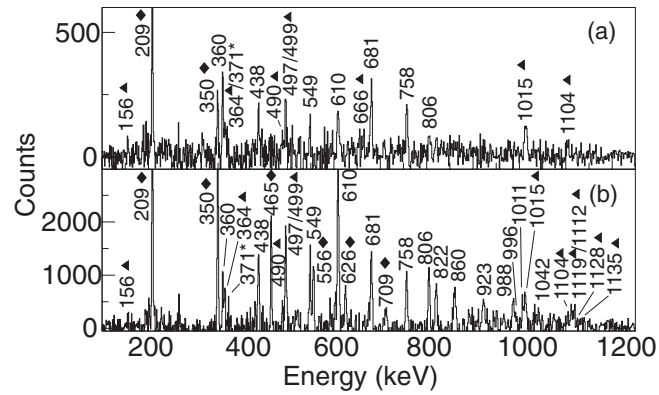

FIG. 8. Background-subtracted γ-ray spectra from the E_γ^4 hypercube for the γ band, produced with a sum of triple gates set on (a) the 438-, 497-, 549-, and 610-keV transitions and (b) the transitions that correspond to the decay of the $21/2^+$ state to the $61/2^+$ state. Photopeaks that correspond to linking transitions are labeled with triangles, photopeaks that correspond to transitions within the yrast band are labeled with diamonds, and the photopeak labeled with an asterisk corresponds to a transition within band 1.

with signature $(+1/2)$. A sum spectrum of triple gates on the low-spin states of this band is presented in Fig. 8(a). Two linking transitions are also identified in this spectrum, which connects the γ band to band 1, as well as a transition of energy 666 keV, which connects the $21/2^+$ state in the γ band to the yrast state with the same spin and parity. The spectrum presented in Fig. 8(b) highlights the high-spin transitions in this band.

E. The strongly-coupled bands

Previously, bands 6 and 7 in Fig. 2 were observed in Refs. [24,25]. The present paper confirms these structures and extends band 6 by two tentative transitions and establishes a new sequence of transitions in parallel with band 7 at high spins. A γ-ray spectrum representative of bands 6 and 7 is presented in Fig. 9, where each panel corresponds to a different energy range. This spectrum confirms the linking transitions that connect bands 6 and 7 to the yrast band and bands 1 and 2, as well as the linking transitions with energies 807 and 929 keV, which infer an excited state at 1713 keV. Angular-intensity ratio measurements for these two transitions were extracted to determine the spin and parity of this level. Both transitions were found to be of a stretched dipole character, which established a spin of 23/2 for this state, although the parity remained undetermined, see the following discussion for a possible positive-parity assignment. Figures 10(a) and 10(b) provide γ-ray spectra that were produced with a sum of triple gates set on the interband transitions between bands 6 and 7 and the intraband transitions from each band. These spectra demonstrate the presence of the highest-spin states in these two bands.

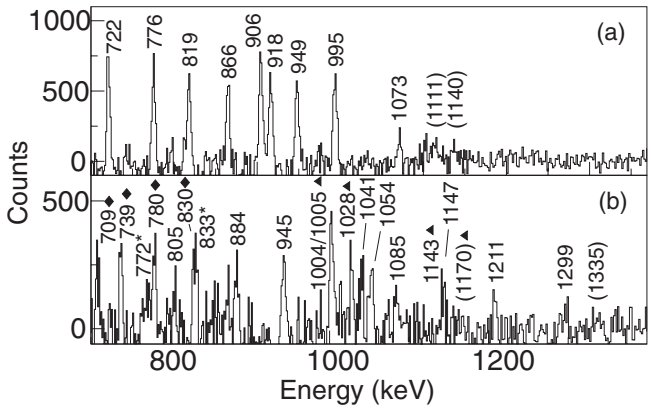

FIG. 7. Background-subtracted γ-ray spectra from the E_γ^4 hypercube produced with a sum of triple gates set on (a) band 4, from the decay of the $33/2^-$ state to the $57/2^-$ state, in coincidence with the 1046-keV transition, and (b) band 10, from the decay of the $59/2^-$ state to the $(91/2^-)$ state. Photopeaks that correspond to linking transitions are labeled with triangles, photopeaks that correspond to transitions within the yrast band are labeled with diamonds, and photopeaks labeled with asterisks correspond to transitions within band 3.

Previously, bands 8 and 9 in Fig. 2 were reported by Simpson *et al.* [25] but were not connected to the main level scheme. In the present paper, a linking transition, which connects band 8 to band 6 has been established. In addition, extensions were possible for both bands 8 and 9. A γ-ray spectrum, which shows the 833-keV linking transition is presented in Fig. 11(a). The low-spin sequences of bands 6 and 7 are present in this spectrum, which confirms that band 6 is linked to band 8 through the $35/2^-$ state. The multipolarity measurement for the 833-keV linking transition suggests that it is of a stretched dipole nature; see Table I. Extensions to the high-spin structure of band 9 can be seen in the γ-ray spectrum presented in Fig. 11(b). In total, three new transitions were observed for band 9 at high spins, which extended this band to a possible $(79/2^+)$ state, and two new transitions were observed for band 8, which extended it to a possible $(73/2^+)$ state. Transitions associated with the low-spin structures of bands 8 and 9 were also observed in the present paper, extending them

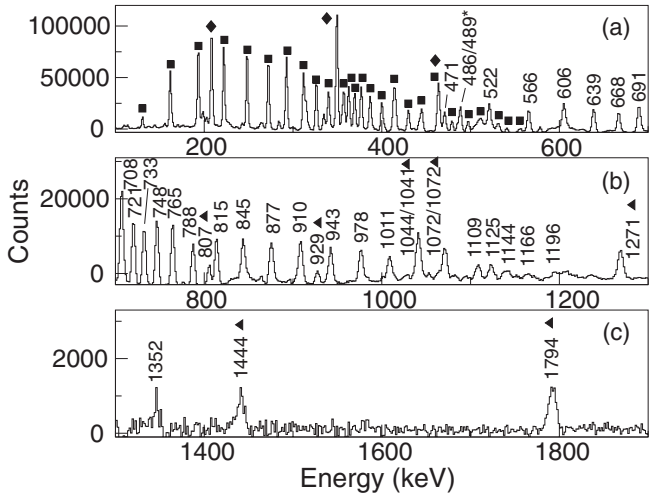

FIG. 9. Background-subtracted γ-ray spectrum from the E_γ^4 hypercube for bands 6 and 7 produced with a sum of triple gates set on the interband transitions. (a) shows the energy range between 100 and 700 keV, (b) shows the energy range between 700 and 1300 keV, and (c) shows the energy range between 1300 and 1900 keV. Photopeaks that correspond to linking transitions are labeled with triangles, photopeaks that correspond to transitions within the yrast band are labeled with diamonds, photopeaks labeled with asterisks correspond to transitions within bands 1 and 2, and photopeaks labeled with squares correspond to the interband transitions between bands 6 and 7.

down to the $(33/2^+)$ and $(31/2^+)$ states, respectively (see the level scheme of Fig. 2 and Table I for details).

A third strongly-coupled structure was observed and tentatively was suggested to be associated with ^{159}Er in Ref. [25]. In this previous paper, the band was interpreted as based on the $\nu h_{11/2}$ [505]11/2 band head from alignment and the $B(M1)/B(E2)$ ratio arguments. This band head is isomeric, and the present data cannot confirm the assignment to ^{159}Er,

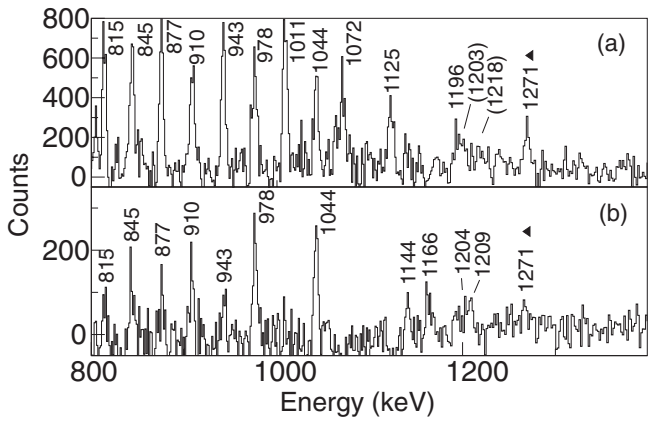

FIG. 10. Background-subtracted γ-ray spectra from the E_γ^4 hypercube for bands 6 and 7 produced with a sum of triple gates set on the interband transitions from 130 to 327 keV and (a) the 1072-, 1125-, and 1196-keV transitions from band 6 and (b) the 1109-keV transition from band 7. Photopeaks that correspond to linking transitions are labeled with triangles.

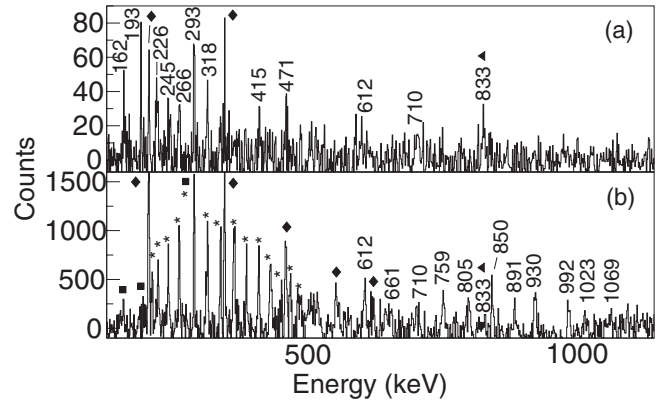

FIG. 11. Background-subtracted γ-ray spectra from the E_γ^4 hypercube for bands 8 and 9. (a) was produced with a triple gate set on the 249- and 272-keV transitions from the decay of bands 6 and 7 and the 215-keV transitions from band 9, and (b) was produced by a sum of triple gates set on all of the interband transitions between bands 8 and 9 in coincidence with the 984-keV transition of band 9. Photopeaks that correspond to linking transitions are labeled with triangles, photopeaks that correspond to transitions within the yrast band are labeled with diamonds, photopeaks labeled with asterisks in (b) correspond to the interband transitions between bands 8 and 9, and photopeaks labeled with squares in (b) correspond to transitions from bands 6 and 7.

therefore, this band has not been included in the present-level scheme. It is noted that the energies of this band at low spin [25] are similar to those in the same structure observed in ^{161}Er [36,37].

IV. DISCUSSION

The odd-N nucleus of $^{159}_{68}\mathrm{Er}_{91}$ has 13 nucleons outside of the doubly magic $^{146}_{64}\mathrm{Gd}_{82}$ core. Its Fermi level lies near the bottom of the $N_{\mathrm{osc}} = 6$ neutron shell. The occupation of the neutron $i_{13/2}$ high-j low-Ω orbitals drives the nuclear shape toward prolate deformation, which gives rise to dominant collective rotational structures. The level schemes of Figs. 1 and 2, constructed from the present paper, provides a diverse range of rotational bands. To determine their underlying configurations, Woods-Saxon cranked shell-model (CSM) calculations [38,39] have been performed for ^{159}Er. The resulting quasiparticle trajectories for the neutrons and protons are presented in Figs. 12(a) and 12(b), respectively. Table II provides the usual labeling scheme for the orbitals involved in the following discussion.

In addition, to help identify the characteristics of the experimentally observed bands in ^{159}Er, aligned angular momentum (or alignment) [40] as a function of rotational frequency and the excitation energy relative to that of a rotating liquid drop (based on the Lublin-Strasbourg model [41,42]) as a function of spin, are plotted in Figs. 13, 15, 16, and 17. In the aligned angular momentum plots, a natural reference [43] was subtracted. This is based on Harris parameters [44,45] extracted from variable moments of inertia fits to the favored ground-state structure (band 2) with values of $\mathcal{J}_0 = 20.4\hbar^2$ MeV^{-1} and $\mathcal{J}_1 = 57.7\hbar^4$ MeV^{-3}.

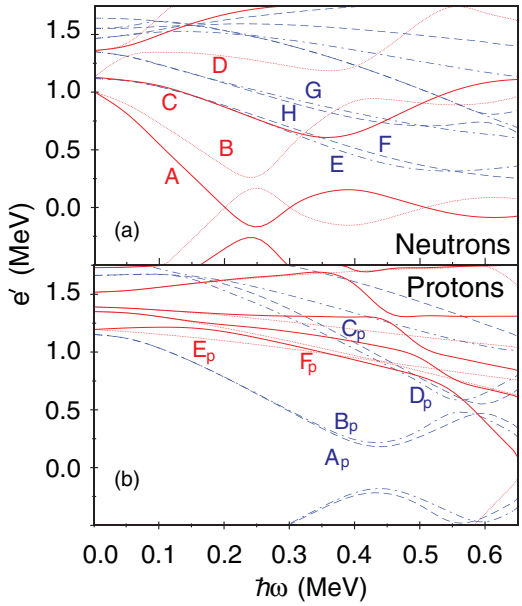

FIG. 12. (Color online) The results of the CSM calculations for ^{159}Er (a) neutrons and (b) protons. The deformation parameters used were $\beta_2 = 0.235$, $\beta_4 = 0.046$, and $\gamma = 0.0^\circ$ and with pair gaps $\Delta_n = 1.00$ MeV and $\Delta_p = 1.13$ MeV. The quasiparticle labeling is given in Table II. Solid lines (red) show levels with parity and signature $(\pi, \alpha) = (+, +1/2)$; dotted lines (red) show $(+, -1/2)$ levels; dashed lines (blue) show $(-, -1/2)$ levels; dot-dashed lines (blue) show $(-, +1/2)$ levels.

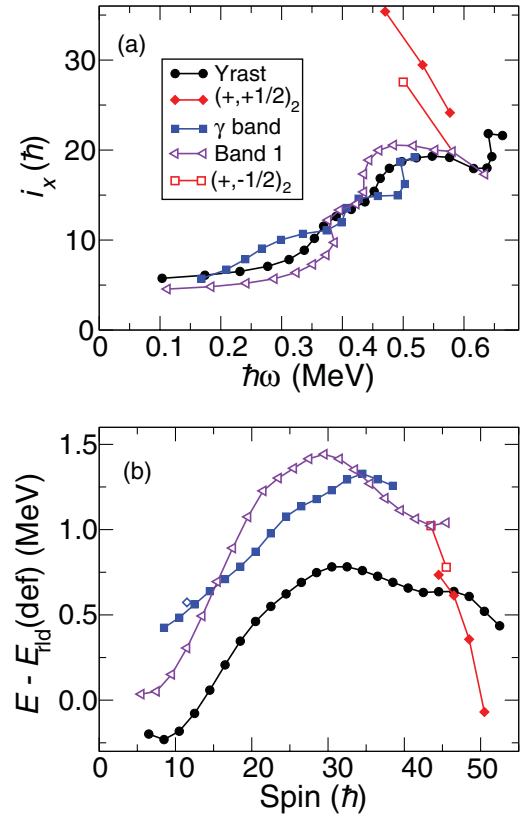

FIG. 13. (Color online) (a) The aligned angular momentum (alignment) as a function of rotational frequency for the yrast band and its high-spin parallel sequence labeled $(+, +1/2)_2$, band 1 and branching above $(87/2^+)$, labeled $(+, -1/2)_2$, and the γ band. (b) Energy relative to a rotating liquid drop as a function of spin for these bands.

The most probable quasiparticle configurations, based on the following discussion, for all of the bands, are summarized in Table III.

A. Positive-parity bands: The yrast band, band 1, and the γ band

Previously, the behavior of the yrast band was discussed [22–24] as based on the odd neutron, which occupied the favored signature $(+, +1/2)$ of the $i_{13/2}$ Nilsson orbital [651]3/2, labeled A in Table II and Fig. 12(a). An initial alignment for this band of $\sim 6\hbar$, from Fig 13(a), reflects its one-quasi-particle nature. With the odd neutron in this active orbital, the first $(i_{13/2})^2$ neutron alignment AB, predicted to occur at $\hbar\omega \sim 0.24$ MeV, is blocked. Instead, this band undergoes the second $(i_{13/2})^2$ neutron alignment BC at $\hbar\omega \sim 0.36$ MeV followed by the first $(h_{11/2})^2$ proton alignment, the A_pB_p crossing, at $\hbar\omega \sim 0.45$ MeV.

TABLE III. A summary of the quasiparticle configurations proposed for the bands observed in ^{159}Er.

Band	Quasiparticle configurations
Yrast	$A \rightarrow ABC \rightarrow ABC \otimes A_pB_p$
1	$B \rightarrow BAD \rightarrow BAD \otimes A_pB_p$ and EF and/or CD
γ band	$\gamma \otimes A \rightarrow \gamma \otimes ABC \rightarrow \gamma \otimes ABC \otimes A_pB_p$
2	$E \rightarrow EAB \rightarrow EAB \otimes A_pB_p$
3	$F \rightarrow FAB \rightarrow FAB \otimes A_pB_p$
4	$GAB \rightarrow GABEF \otimes A_pB_p$
5	$EBC \rightarrow EBC \otimes A_pB_p$
6 and 7	$A \otimes A_pE_p(F_p) \rightarrow ABC \otimes A_pE_p(F_p)$
8 and 9	$EAB \otimes A_pE_p(F_p) \rightarrow EAB \otimes A_pE_p(F_p)B_pC_p$ and A_pD_p
10	$(HABEF) \rightarrow (HABEF \otimes A_pB_p)$

Band 1 has been established as the unfavored signature partner of the yrast structure $(+, -1/2)$ [22], with the odd neutron occupying the B orbital of Table II and Fig. 12(a). The alignment and energy of this band, Fig. 13, show it to have a lower initial alignment than the yrast band and to lie higher in energy. The present paper has pushed this band from the $43/2^+$ state up to high spin $(91/2^+)$, and the alignment plot in Fig. 13(a) establishes two gains in alignment at $\hbar\omega \sim 0.38$ and $\hbar\omega \sim 0.44$ MeV. The first gain is interpreted as the third $(i_{13/2})^2$ neutron alignment AD, and the second is interpreted as the A_pB_p crossing.

The new band observed in the present paper, labeled the γ band in Fig. 2, is at a higher-excitation energy but has the same parity and signature as the yrast band. A possible interpretation for this sequence is that it is based on a vibrational excitation coupled to the $i_{13/2}$ neutron yrast band. The systematics for the first few states of the bands based on γ-vibrational excitations in the erbium isotopes with $N = 88$ through to $N = 94$ are presented in Fig. 14. The energy of the corresponding yrast

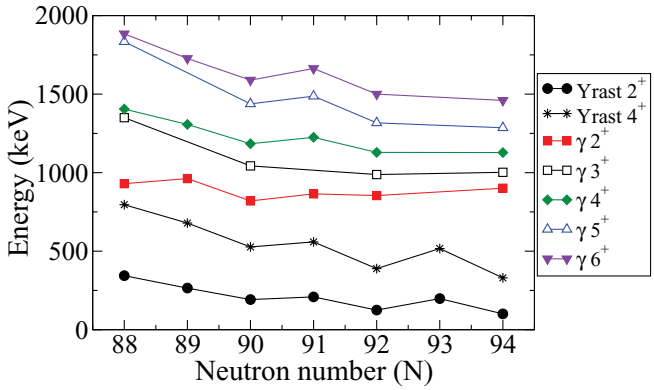

FIG. 14. (Color online) Systematics for the 2^+, 3^+, 4^+, 5^+, and 6^+ states of the bands based on γ-vibrational excitations for ^{156}Er [46], ^{157}Er [3], ^{158}Er [22], ^{159}Er, ^{160}Er [47], and ^{162}Er [48]. Also included are the values for the yrast 2^+ and 4^+ states. The energies and spins of the bands observed in the odd-A isotopes are given relative to the lowest-lying state of the yrast band with $13/2^+$.

2^+ and 4^+ states are also presented in this figure. For the odd-A erbium isotopes, the energies and spins have been plotted relative to the yrast $13/2^+$ state. The level energies for the γ band in ^{159}Er exhibit good agreement with the systematics for the corresponding states identified in these neighboring isotopes and, therefore, may be interpreted as based on the γ-vibrational excitation at low spins. At higher spins, the plots of Fig. 13 show a more complex nature for this band. Two gains in alignment are observed with increasing angular frequency at $\hbar\omega \sim 0.40$ and $\sim$0.50 MeV, which are interpreted as delayed BC and A_pB_p crossings, respectively. The nature of the upturn in alignment between $\hbar\omega \sim 0.20$ MeV and $\sim$0.35 is unclear.

Also plotted in Fig. 14 are the energies of the 3^+ and 5^+ odd-spin γ-vibrational states observed in the even-even isotopes. A possible candidate for the corresponding state in ^{159}Er is the $23/2^{(+)}$ state (plotted in Fig. 14), which is associated with the decay out of band 7 in Fig. 1. This state is also plotted in the energy plot of Fig. 13(b) as an open diamond.

B. Negative-parity bands: Bands 2, 3, 4, 5, and 10

Previously, bands 2 and 3 were interpreted as based on the [521]3/2 Nilsson orbital with $(-,+1/2)$ and $(-,-1/2)$ [22,24], the E and F configurations, respectively. With the addition of the new transitions observed in the present paper for band 3 between the $15/2^-$ and $27/2^-$ states, both signature partners are observed to undergo the AB crossing at $\hbar\omega \sim$ 0.24 MeV; see Fig. 15(a). At higher angular frequency, $\hbar\omega \sim$ 0.42 MeV, both bands experience the first $(h_{11/2})^2$ proton alignment A_pB_p [24].

Previously, band 4 was discussed in terms of the next higher-lying negative-parity positive-signature configuration G [24]. Its initial alignment, from the plot of Fig. 15(a), of $\sim 8\hbar$ at $\hbar\omega \sim 0.24$ MeV suggests the configuration GAB. This band then appears to experience a gradual gain in alignment with increasing angular frequency. A more distinct gain in alignment occurs at $\hbar\omega \sim 0.45$ MeV, which is most likely the A_pB_p crossing. After this crossing, its alignment is $\sim 2\hbar$ higher

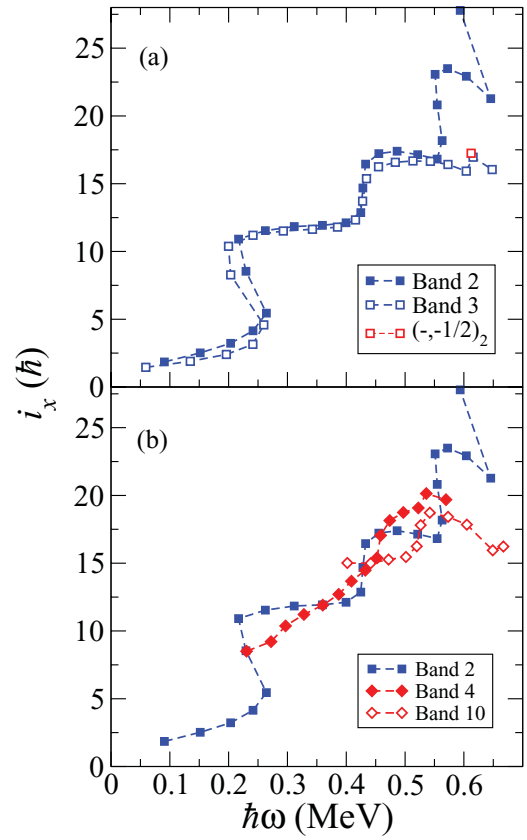

FIG. 15. (Color online) The aligned angular momentum (alignment) as a function of rotational frequency for band 2 with (a) band 3 and its high-spin parallel sequence labeled $(-,-1/2)_2$ and (b) bands 4 and 10.

than that of bands 2 and 3 (based on the E and F configurations at low frequency, respectively). A possible reason for this may lie with the $(f_{7/2}/h_{9/2})^2$ EF crossing, which occurs at roughly the same rotational frequency as the A_pB_p crossing.

The negative-parity positive-signature nature of band 5 suggests that it is associated with either the next higher-lying configuration above G or that it corresponds to a continuation of the E configuration beyond the AB crossing. The latter interpretation was speculated in Ref. [24]. With the addition of the new transitions observed in the present paper, the alignment characteristics lend weight to this assignment, with the initial alignment that suggests a smooth continuation of the E configuration, which possibly undergoes a second $(i_{13/2})^2$ neutron alignment (BC) at $\hbar\omega \sim 0.27$ MeV and the proton A_pB_p alignment at $\hbar\omega \sim 0.38$ MeV; see Fig. 16(a).

In the present paper, a new band with negative parity and negative signature has been observed, band 10. This assignment would suggest that band 10 is the signature partner of either band 4 or band 5. The alignment and energy plots of Figs. 15(a) and 15(b) do not give a clear indication as to which interpretation is most likely. However, band 4 lies at a lower excitation energy than band 5, and therefore, band 10 may be its unfavored signature partner. The initial alignment of band 10 of $\sim 15\hbar$ suggests that it is based on, at least, a three- or five-quasi-particle configuration. The alignment

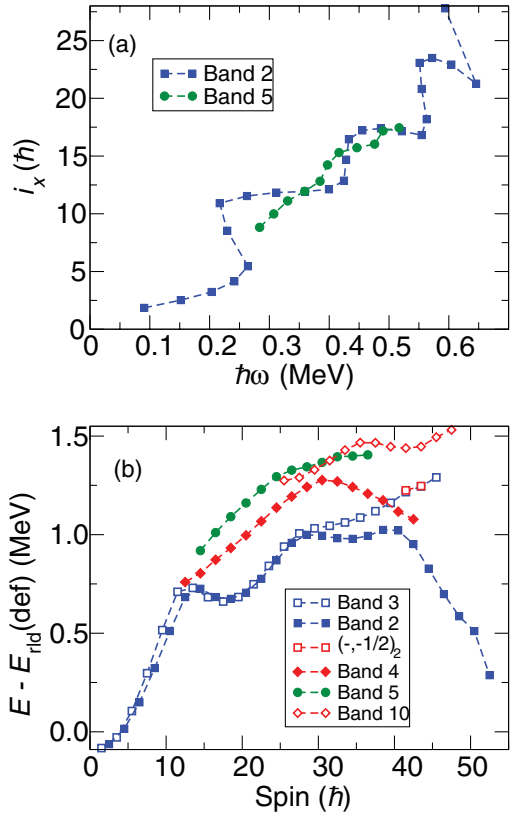

FIG. 16. (Color online) (a) The aligned angular momentum (alignment) as a function of rotational frequency for bands 2 and 5. (b) Energy relative to a rotating liquid drop as a function of spin for bands 2, 3 [with its high-spin parallel sequence $(-, -1/2)_2$], 4, 5, and 10.

gain at $\hbar\omega \sim 0.52$ MeV may also be attributed to a further two-quasi-particle excitation. If band 10 is interpreted as the unfavored signature partner of band 4, then its initial alignment may be attributed to the $HABEF$ configuration, which then undergoes a delayed A_pB_p crossing at $\hbar\omega \sim 0.52$ MeV. The latter crossing may also be an unpaired band crossing that involves a pair of neutrons as discussed in Sec. IV D. However, in the absence of the low-spin structure of this band, these assignments remain speculative.

C. Strongly-coupled structures

The strongly-coupled signature-partner bands observed in ^{159}Er were discussed previously in terms of multiquasi-particle excitations that involved the $\pi h_{11/2}[523]7/2$ and $\pi g_{7/2}[404]7/2$ configurations coupled to the odd neutron [25]. Branching ratios were measured, and ratios of reduced transition probabilities $B(M1)/B(E2)$ were deduced, which strengthened the proposed assignments.

Bands 6 and 7 (labeled band 1 in the previous paper of Ref. [25]) were interpreted at low rotational frequency as the $A \otimes A_pE_p(F_p)$ configurations. The gain in alignment at $\hbar\omega \sim 0.34$ MeV, see Fig. 17(a), then was attributed to the BC crossing. In the present paper, the strongly-coupled sequence, bands 6 and 7, has been extended up to higher spins, and an additional sequence has been observed in parallel with band 7. With the extensions to band 6, a gain in alignment is observed at $\hbar\omega \sim 0.59$ MeV. At a similar frequency in band 7, the alignment becomes somewhat erratic, and the parallel sequence is observed. The second and third proton alignments, the B_pC_p and A_pD_p crossings, respectively, are predicted to occur around this angular frequency, see Fig. 12, and may be the cause of these observations.

Previously, the second strongly-coupled structure, bands 8 and 9, was discussed in terms of the $A_pE_p(F_p)$ configuration coupled to the odd neutron that resides in the E orbital and, therefore, by assigning positive parity to the band [25] (labeled band 2 in this previous paper). The spin assignments deduced for these bands suggested that an initial configuration of $EAB \otimes A_pE_p(F_p)$ was appropriate for the alignment. From the present paper, the addition of the observed connecting transition and its measured dipole nature helps to confirm the previously deduced spin assignments. The band-head spins for bands 8 and 9 are assigned $(33/2^+)$ and $(31/2^+)$, respectively, in agreement with Ref. [25]. The newly observed extensions at low spins for these bands also help to confirm the previous configuration assignment with a sharp gain in alignment in the plot of Fig. 17(a) at $\hbar\omega \sim 0.22$ MeV, which suggests the presence of the AB crossing. The extensions at high spin show gains in alignment for both bands at $\hbar\omega \sim 0.48$ MeV; see Fig. 17(a). As with bands 6 and 7, the A_pB_p crossing is expected to be blocked in bands 8 and 9 caused by the presence

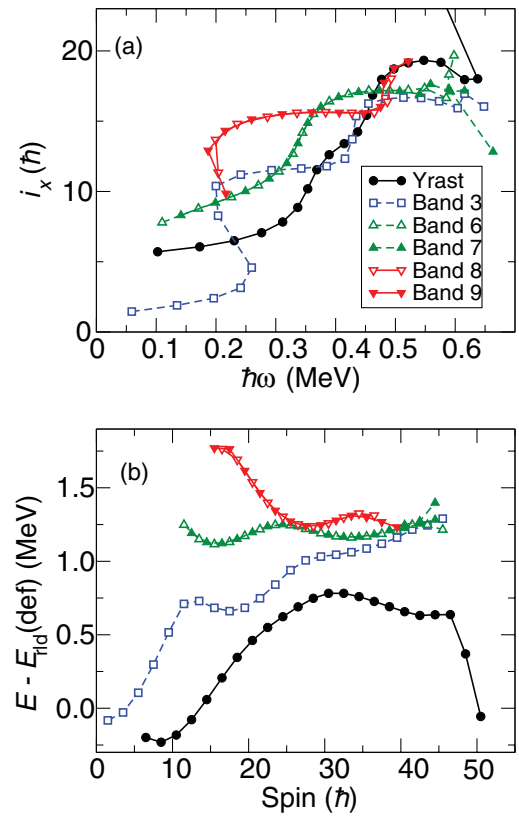

FIG. 17. (Color online) (a) The aligned angular momentum (alignment) as a function of rotational frequency for the strongly coupled bands. (b) Energy relative to a rotating liquid drop as a function of spin for these bands. See text for further details.

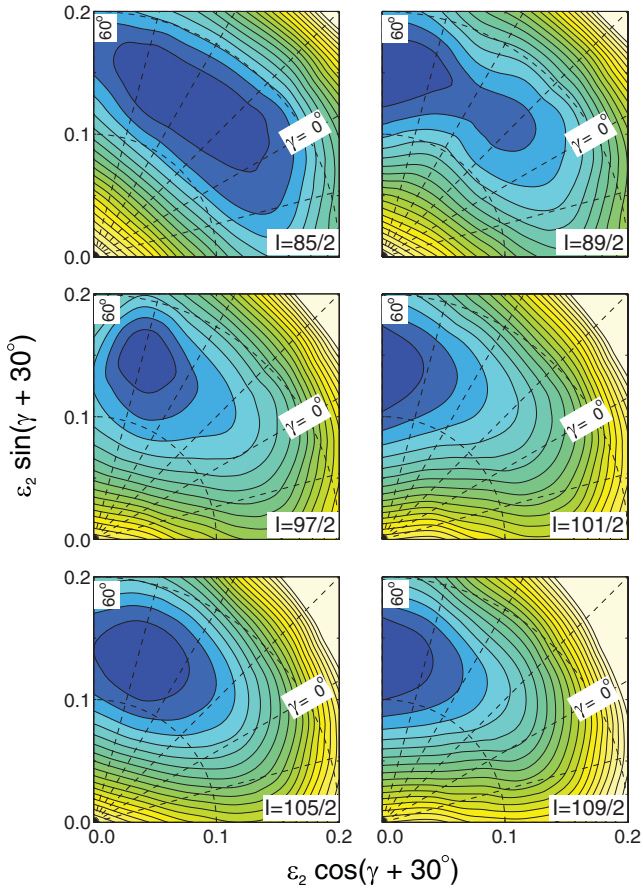

FIG. 18. (Color online) Calculated energy as a function of the shape of the nuclear potential. The potential is specified by using the quadrupole deformation parameter ε_2 and the triaxiality parameter γ. The energy surfaces are drawn for the $(+,+1/2)\pi(h_{11/2})^4\nu(i_{13/2})^3$ configuration of ^{159}Er at spins 85/2, 89/2, 97/2, 101/2, 105/2, and 109/2. Contour lines are separated by 0.25 MeV, and the γ plane is marked at 15° intervals. Dark regions represent low energy.

of a proton in the A_p orbital. Therefore, these alignment gains could be attributed to the B_pC_p and A_pD_p crossings. The crossings appear lower in angular frequency than predicted by the CSM calculations, Fig. 12(b), which may be an indication that these configurations have different deformations. It is interesting to note that the unpaired band crossings, attributed to the specific neutron $i_{13/2}$ single-particle exchanges in band 2, see discussion in Sec. IV D, may well be expected in these strongly coupled bands since they are based on the same neutron configuration.

D. Band termination, oblate structures, and unpaired band crossings

At the highest spins in the yrast band, a parallel γ-decay sequence is observed from a second $I^\pi = 89/2^+$ state and is labeled $(+,+1/2)_2$ in Fig. 13. This sequence quickly becomes yrast, see Fig. 13(b), and extends up to the $(101/2^+)$ state. In Ref. [26], it was suggested that the structure of the $89/2^+$ and $(101/2^+)$ states, in this decay sequence, is similar to the favored oblate configurations at 40^+ and 46^+ in ^{158}Er [12].

To understand the behavior of ^{159}Er at the highest angular momenta observed, calculations have been performed using the unpaired CNS model [42,49,50]. In this formalism, configurations are specified by the total number of particles in the open j shells (or valence shells) contrary to the CSM formalism where only aligned particles are listed. In the CNS formalism, some of the measured yrast $(+,+1/2)$ states are interpreted as being built with four $h_{11/2}$ proton orbitals and three $i_{13/2}$ neutron orbitals occupied outside the $^{146}_{64}$Gd$_{82}$ core. Potential energy surfaces for this configuration are presented in Fig. 18. This $\pi(h_{11/2})^4\nu(i_{13/2})^3$ configuration starts out with a near-prolate shape ($\gamma = 0°$), and, as shown in Fig. 18, it is still collective at $85/2^+$ but with $\gamma \sim 35°$. At higher spins, well-defined minima with $\gamma = 60°$ (noncollective oblate) are predicted to occur at $89/2^+$, $101/2^+$, and $109/2^+$. The $\gamma = 60°$ minimum at $101/2^+$ corresponds to a terminating state, which is constructed from full alignment of the spin vectors in the valence configuration $[\pi(h_{11/2})^4]_{16^+}[\nu(i_{13/2})^3(h_{9/2}f_{7/2})^6]_{69/2^+}$. This is similar to the configuration for the fully aligned 46^+ state in neighboring ^{158}Er but with the extra odd neutron that resides in the next available $i_{13/2}$ orbital for ^{159}Er [26]. Similarly, the $89/2^+$ state with $\gamma = 60°$ is constructed with one spin vector of the $h_{9/2}f_{7/2}$ neutrons antialigned. The fully aligned $101/2^+$ state is illustrated in a sloping Fermi surface diagram in Fig. 19. By starting from this state, an arrow illustrates how the $89/2^+$ state is formed when one neutron is moved within the $h_{9/2}f_{7/2}$ orbitals from an $m = 5/2$ state to an $m = -7/2$ state. Similarly, a $(+,-1/2)$ $91/2^+$ state is formed when the neutron is moved from the $m = 5/2$ state; see Fig. 19.

The energies for the configurations calculated in the yrast region above spin $30\hbar$ are presented with the experimental data in Fig. 20. The positive- and negative-parity states are shown in the left and right panels, respectively. The $(+,+1/2)_2$ sequence (89/2–101/2) with the aligned states at $89/2^+$ and $(101/2^+)$ is described well by the $\pi(h_{11/2})^4\nu(i_{13/2})^3$ configuration, which is illustrated in Fig. 18. The $(+,+1/2)$ yrast states for $I \leqslant 89/2$ are interpreted as being built on a configuration with two additional $h_{11/2}$ protons, namely, $\pi(h_{11/2})^6\nu(i_{13/2})^3$. The difference in the slopes of the experimental and calculated $E - E_{\rm rld}$ curves for spin values $I \approx 30$–40 may be explained from pairing correlations that are not included in the calculations.

It is possible to build higher-spin states than $101/2^+$ within the constraints of the $\pi(h_{11/2})^4\nu(i_{13/2})^3$ configuration. This is achieved by promoting a proton from the $d_{5/2}g_{7/2}$ orbitals to the $d_{3/2}s_{1/2}$ orbitals, which forms a new rotational band that terminates at $109/2^+$. The formation of this $109/2^+$ state is also illustrated in Fig. 19, i.e., by starting from the aligned $101/2^+$ state, a proton is moved within the $N_{\rm osc} = 4$ orbitals from an $m = -5/2$ state below the $Z = 64$ gap to the $m = 3/2$ state above the gap. This terminating state has yet to be observed experimentally. However, the higher-spin states in the continuation of the yrast band above $89/2^+$ might be built with this configuration; see Fig. 20(b).

The $(+,-1/2)$ states (band 1) branch at $(87/2^+)$; see Figs. 1 and 20(a). The lowest-energy branch appears to be

similar to that observed in the yrast band, which suggests that the lowest-energy $(91/2^+)$ state is the aligned configuration $[\pi(h_{11/2})^4]_{16^+}[\nu(i_{13/2})^3(h_{9/2}f_{7/2})^6]_{59/2^+}$. This configuration is illustrated in the sloping Fermi surface diagram, Fig. 19. The observation of this state supports the prediction [14] that an aligned state should be observed in the neighboring nucleus of ^{158}Er at 41^+. This state, with the configuration $[\pi(h_{11/2})^4]_{16^+}[\nu(i_{13/2})^2(h_{9/2}f_{7/2})^6]_{25^+}$, is yet to be observed experimentally.

For negative parity at high spin, configurations with an odd number of $h_{11/2}$ protons and $i_{13/2}$ neutrons are favored in the calculations; see Fig. 20(e). For signature $\alpha = 1/2$, these configurations also give a possible explanation for crossings observed in band 2. A problem, however, is that the signature $\alpha = -1/2$ branch, not shown in Fig. 20(e), is calculated to lie ∼150 keV lower in energy in the $I = 40$–50 spin range. Although these configurations are lowest in energy, they are not assigned to the observed bands 2 and 3. This is because these bands are interpreted, at intermediate spin values in the paired regime, as having negative parity for the neutrons, according to the above discussion of their alignment properties and comparison with the CSM. Therefore, band 2 is assigned to configurations with an even number of both $h_{11/2}$ protons and $i_{13/2}$ neutrons, which are also shown in Fig. 20(e). The crossing observed at $I \approx 40$ is understood as arising between bands based on configurations with two and four $i_{13/2}$ neutrons [which are labeled [6(1),2] and [6(1),4], respectively, in Fig. 20(e)]. Indeed, the observation of an isolated band crossing at this frequency in the experimental data led Riley *et al.* [29] to interpret this as an unpaired band crossing. This crossing was described as an exchange of occupation at the crossing of a pair of high-j $(i_{13/2})$ neutrons. The scenario of such a crossing, which occurs independently of pairing, is thus supported by the present CNS calculations.

The unpaired band crossing in band 2 occurs at a frequency $\hbar\omega \sim 0.55$ MeV. The simple single-particle model, outlined in Ref. [29], predicted a similar crossing in band 3 but at a higher rotational frequency. The new high-spin transitions in band 3 indicate a branching in the sequence at $79/2^-$ with $\hbar\omega \sim 0.60$ MeV; see Fig. 1, which may indicate a crossing. The additional $(83/2^-)$, $(87/2^-)$ states have very similar energies to corresponding states in band 3, as presented in Fig. 1 and Table I. The CNS calculations also predict a delayed crossing between configurations with two and four $i_{13/2}$ neutrons in this $\alpha = -1/2$ branch but at a spin value, which roughly coincides with the highest observed spin in band 3. This suggests that band 3 needs to be observed for higher-spin values to test these predictions.

At the highest-spin values in band 2, another discontinuity is observed experimentally. This correlates well with the calculated crossing between configurations with six and four $h_{11/2}$ protons; see Fig. 20(e). Then, this would suggest that the highest-spin state of band 2 $(105/2^-)$ corresponds to the full spin alignment in the valence space configuration $[\pi(h_{11/2})^4]_{16^+}[\nu(i_{13/2})^4(h_{9/2}f_{7/2})^5]_{73/2^-}$. In the calculations, the relative energies are off by approximately 500 keV, but this is not unexpected for configurations that differ by a two-particle two-hole excitation.

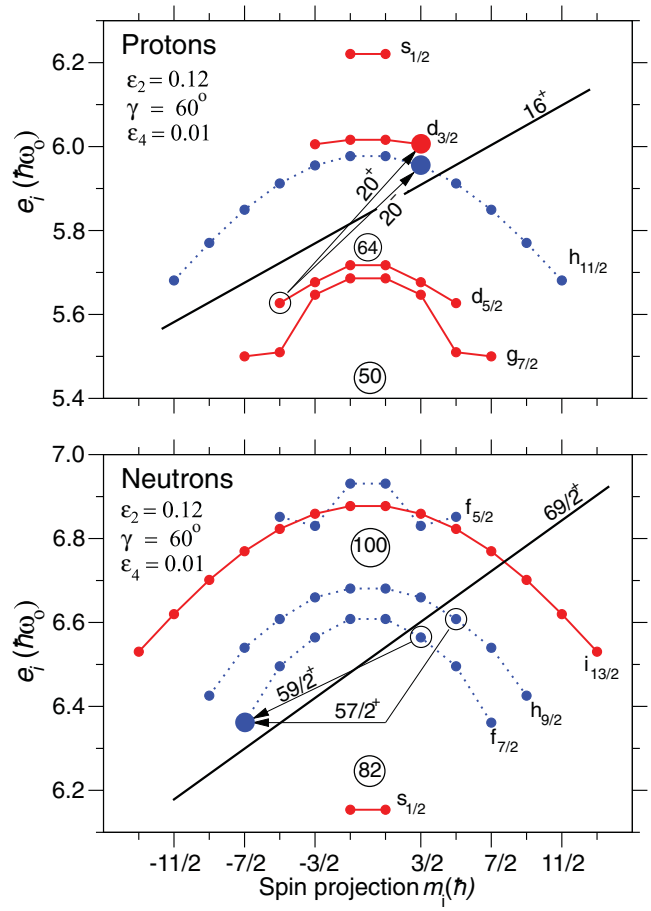

FIG. 19. (Color online) Sloping Fermi surface diagrams for protons and neutrons at the deformation specified in the figure, which is typical for the terminating configurations in ^{159}Er. The orbitals are labeled by subshells, but some of these subshells are strongly mixed so that, for example, the neutron $h_{9/2}f_{7/2}$ or the proton $g_{7/2}d_{5/2}$ orbitals are treated as one entity. In the fully aligned proton 16^+ state and neutron $69/2^+$ state, all orbitals below the sloping Fermi surfaces drawn by thick lines are occupied. Then, how favored lower spin-aligned states can be formed if one neutron is moved to an antialigned orbital and how higher spin favored states are formed when one proton is excited across the $Z = 64$ gap are indicated by arrows. With the present $A = 150$ parameters [51], the $m = \pm 1/2$ and $m = \pm 3/2$ states of the proton $h_{11/2}$ subshell and those labeled $d_{3/2}$ are very close to degenerate. Therefore, the $d_{3/2}$ states are drawn at a somewhat higher energy to make the figure easier to read.

The interpretation, at high spins, of the positive-parity yrast band and band 1 with the aligned states at $89/2$, $91/2$, and $101/2$, together with the negative-parity band 2, appear successful. Indeed, the difference in energy between the $89/2^+$ and $101/2^+$ states experimentally is 3.16 MeV, whereas, the calculations give 2.96 MeV. At such high spins and excitation energies, this agreement, to within a few hundred keV, is satisfactory. The energy difference between experiment and theory for the analogous states in ^{158}Er, namely, the 40^+ and 46^+ states, was discussed previously in Ref. [52].

An interesting observation is that the energy difference between the states in the yrast band and band 1 is approximately 0.5 MeV in the high-spin range, whereas, these bands are

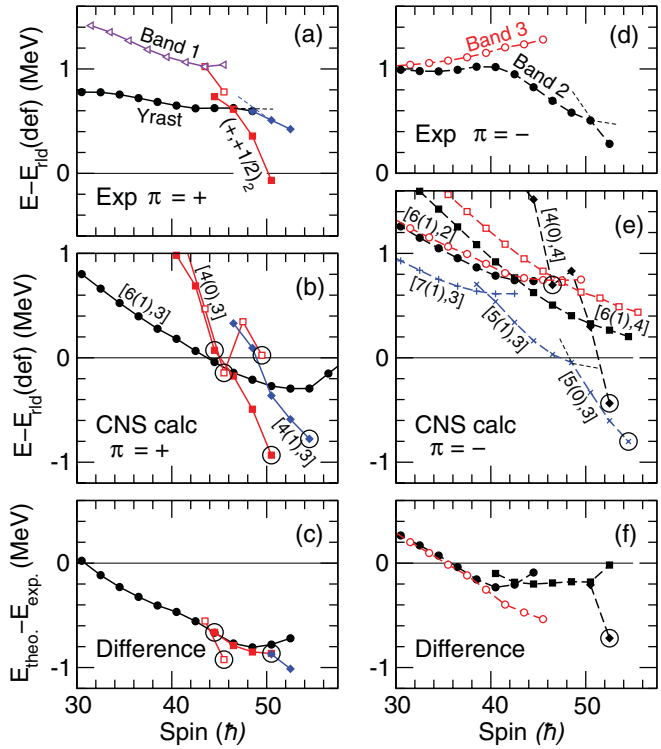

FIG. 20. (Color online) Experimental and calculated energies relative to a rotating liquid drop as a function of spin for the near-yrast bands above 30$\hbar$. (a) and (b) are positive-parity states. (d) and (e) are negative-parity states. The energy difference between the experimental states and the associated calculated states assigned by theory is presented in (c) and (f) for the positive- and negative-parity states, respectively. The calculated configurations are labeled in the standard way by the number of $h_{11/2}$ protons and $i_{13/2}$ neutrons but, in addition, by the number of $d_{3/2}s_{1/2}$ protons in parentheses. Positive-parity states are connected by solid lines, and negative-parity states are connected by broken lines. Solid symbols correspond to ($\alpha = +1/2$), and open symbols correspond to ($\alpha = -1/2$). Aligned states are marked with large open circles. Suggested band crossings are indicated by thin dashed lines. Note that the differences in panel (f) are obtained when the negative-parity bands 2 and 3 are compared with configurations that are calculated a few hundred keV above yrast; see text for details.

close to degenerate in the unpaired CNS calculations. The reason for this signature doubling, which is not observed in the experiment, is that these configurations with an even number of $h_{11/2}$ protons have one $d_{3/2}s_{1/2}$ proton (as seen from the configuration labels in Fig. 20) and, thus, one or three holes in the $g_{7/2}d_{5/2}$ orbitals below the $Z = 64$ gap. At prolate shape, they are the [404]7/2 and [402]5/2 Nilsson orbitals, which are both close to signature degenerate; see, e.g., Fig. 3 of Ref. [13]. From the general experience of pairing correlations in the ground state, both these configurations can be described as having a broken pair, and it might then be assumed that they have similar pairing energies. To investigate this, preliminary calculations, which include pairing, have been performed according to the formalism presented in Ref. [53], i.e., with particle-number projection and minimization of the energy not only in the shape degrees of freedom, but also in the pairing gap Δ and Fermi energy λ. The outcome is that, in general agreement with the experiment, the configuration with the same number of protons in both signatures is favored by approximately 0.5 MeV compared with the configuration with two odd protons, which have the signature $\alpha = -1/2$. Thus, it appears that, in this high-spin region, the combination of an $\alpha = -1/2$ proton of $d_{3/2}s_{1/2}$ character with an $\alpha = +1/2$ proton of $g_{7/2}d_{5/2}$ character has a lower pairing energy than the combination where the signatures are the same. Since, at zero rotation, this would not be the case, this demonstrates the different mixtures of the wave functions in the high-spin region.

E. Triaxial bands

Beyond the terminating states at $\sim 40\hbar$ in ^{157,158}Er, collective bands with high moments of inertia have been observed [15]. Bands with similar characteristics were observed in the present experiment for ^{159}Er and ^{160}Er [20]. These bands have been compared with CNS calculations and have been interpreted as TSD structures [20] $\varepsilon_2 \sim 0.37$ and $\gamma \sim \pm 20^\circ$. The possible TSD band associated with ^{159}Er is labeled TSD 1 in Fig. 1 and has been assigned tentative spin values based on comparisons with CNS calculations [20]. Lifetime measurements on the bands in ^{157,158}Er [16] confirm that these bands are indeed strongly deformed. However, the experimentally extracted Q_t values do not agree with the calculated favored triaxial minimum, which has positive γ deformation. In fact, a more deformed positive-γ or a negative-γ deformation gives better agreement. These recent experimental results highlight a challenge for the understanding of the triaxial degree of freedom and suggest that other theoretical approaches may need to be explored [16]. Indeed, tilted cranking models suggest that the rotational axis can lie between the intermediate and the short principal axes. Thus, a rotational band may be associated with a mixing of the positive- and negative-γ minima, and recent calculations by Shi *et al.* [54] discuss this issue and the structures responsible for the reemergence of collectivity at such high-spin values ($I = 50$–$60\hbar$).

V. CONCLUSIONS

A detailed spectroscopic investigation of ^{159}Er has been performed to understand the structural changes that occur with increasing angular momentum and excitation energy. The paper has revealed new rotational bands and extensions to existing ones, which are based on specific quasiparticle configurations discussed within the framework of the CSM. In addition, one new band may be based on the γ-vibrational structure coupled to the $i_{13/2}$ yrast band. At the highest spins observed, $\sim 50\hbar$, there is strong evidence for yrast and near-yrast terminating sequences, which signify a change in structure from collective prolate to single-particle oblate shapes. Indeed, the favored positive-parity states at $89/2^+$, $91/2^+$, and $(101/2^+)$ and the negative-parity $(105/2^-)$ state, are interpreted as the fully aligned terminating states from comparisons with CNS calculations. The unpaired band crossing at $\hbar\omega = 0.55$ MeV in band 2, identified previously, is confirmed in the CNS

calculations. A band with a high moment of inertia was also observed and was interpreted as a strongly deformed triaxial structure, although the exact nature of the γ deformation remains to be understood.

ACKNOWLEDGMENTS

The authors thank Paul Morrall for preparing the targets and the ATLAS operations staff for assistance. This work has been supported, in part, by the US National Science Foundation under Grants No. PHY-0756474 (FSU) and No. PHY-0554762 (USNA) and the US Department of Energy, Office of Nuclear Physics, under Contracts No. DE-AC02-06CH11357 (ANL), No. DE-FG02-94ER40834 (UMD), No. DE-AC02-05CH11231 (LBNL), and No. DE-FG02-96ER40983 (UTK), the United Kingdom Science and Technology Facilities Council, the Swedish Science Research Council, and by the State of Florida.

[1] J. Simpson *et al.*, Phys. Rev. Lett. **53**, 648 (1984).
[2] P. O. Tjøm, R. M. Diamond, J. C. Bacelar, E. M. Beck, M. A. Deleplanque, J. E. Draper, and F. S. Stephens, Phys. Rev. Lett. **55**, 2405 (1985).
[3] S. J. Gale *et al.*, J. Phys. G **21**, 193 (1995).
[4] F. S. Stephens, M. A. Deleplanque, R. M. Diamond, A. O. Macchiavelli, and J. E. Draper, Phys. Rev. Lett. **54**, 2584 (1985).
[5] H. W. Cranmer-Gordon *et al.*, Nucl. Phys. A **465**, 506 (1987).
[6] H. Emling *et al.*, Phys. Lett. B **217**, 33 (1989).
[7] J. D. Morrison, J. F. Sharpey-Schafer, M. A. Bentley, H. W. Cranmer-Gordon, P. Fallon, P. D. Forsyth, D. Howe, A. R. Mokhtar, M. A. Riley, and J. Simpson, Europhys. Lett. **6**, 493 (1988).
[8] C. Baktash *et al.*, Phys. Rev. Lett. **54**, 978 (1985).
[9] T. Byrski *et al.*, Nucl. Phys. A **474**, 193 (1987).
[10] J. Burde, E. L. Dines, S. Shih, R. M. Diamond, J. E. Draper, K. H. Lindenberger, C. Schück, and F. S. Stephens, Phys. Rev. Lett. **48**, 530 (1982).
[11] M. A. Riley, J. D. Garrett, J. F. Sharpey-Schafer, and J. Simpson, Phys. Lett. B **177**, 15 (1986).
[12] I. Ragnarsson, Z. Xing, T. Bengtsson, and M. A. Riley, Phys. Scr. **34**, 651 (1986).
[13] T. Bengtsson and I. Ragnarsson, Phys. Scr., T **5**, 165 (1983).
[14] J. Simpson *et al.*, Phys. Lett. B **327**, 187 (1994).
[15] E. S. Paul *et al.*, Phys. Rev. Lett. **98**, 012501 (2007).
[16] X. Wang *et al.*, Phys. Lett. B **702**, 127 (2011).
[17] A. Aguilar *et al.*, Phys. Rev. C **77**, 021302 (2008).
[18] C. Teal *et al.*, Phys. Rev. C **78**, 017305 (2008).
[19] N. S. Pattabiraman *et al.*, Phys. Lett. B **647**, 243 (2007).
[20] J. Ollier *et al.*, Phys. Rev. C **80**, 064322 (2009).
[21] J. Ollier *et al.*, Phys. Rev. C **83**, 044309 (2011).
[22] J. Simpson, P. A. Butler, P. D. Forsyth, J. F. Sharpy-Schafer, J. D. Garrett, G. B. Hagemann, B. Herskind, and L. P. Ekstrom, J. Phys. G **10**, 383 (1984).
[23] J. Simpson *et al.*, J. Phys. G **13**, 847 (1987).
[24] M. A. Deleplanque, J. C. Bacelar, E. M. Beck, R. M. Diamond, J. E. Draper, R. J. McDonald, and F. S. Stephens, Phys. Lett. B **193**, 422 (1987).
[25] J. Simpson *et al.*, Eur. Phys. J. A **1**, 267 (1998).
[26] F. G. Kondev *et al.*, J. Phys. G **25**, 897 (1999).
[27] R. Bengtsson and S. Frauendorf, Nucl. Phys. A **327**, 139 (1979).
[28] R. Bengtsson and S. Frauendorf, Nucl. Phys. A **314**, 27 (1979).
[29] M. A. Riley, J. D. Garrett, J. Simpson, and J. F. Sharpey-Schafer, Phys. Rev. Lett. **60**, 553 (1988).
[30] I. Y. Lee, Nucl. Phys. A **520**, c641 (1990).
[31] R. V. F. Janssens and F. S. Stephens, Nucl. Phys. News **6**, 9 (1996).
[32] D. C. Radford, Nucl. Instrum. Methods Phys. Res. A **361**, 297 (1995).
[33] D. C. Radford, M. Cromaz, and C. J. Beyer, in *Proceedings of the Nuclear Structure '98 Conference, Gatlinburg, 1998*, edited by C. Baktash (American Institute of Physics, College Park, MD, 1999), p. 570.
[34] C. W. Beausang, D. Prevost, M. H. Bergstrom, G. de France, B. Haas, J. C. Lisle, C. Theisen, J. Timár, P. J. Twin, and J. N. Wilson, Nucl. Instrum. Methods Phys. Res. A **364**, 560 (1995).
[35] L. P. Ekström and A. Nordlund, Nucl. Instrum. Methods Phys. Res. A **313**, 421 (1992).
[36] J. D. Garrett, G. B. Hagemann, B. Herskind, J. Bacelar, R. Chapman, J. C. Lisle, J. N. Mo, A. Simcock, J. C. Willmott, and H. G. Price, Phys. Lett. B **118**, 297 (1982).
[37] L. Chen *et al.*, Phys. Rev. C **83**, 034318 (2011).
[38] W. Nazarewicz, J. Dudek, R. Bengtsson, T. Bengtsson, and I. Ragnarsson, Nucl. Phys. A **435**, 397 (1985).
[39] S. Cwiok, J. Dudek, W. Nazarewicz, W. Skalski, and T. Werner, Comput. Phys. Commun. **46**, 379 (1987).
[40] R. Bengtsson, S. Frauendorf, and F.-R. May, At. Data Nucl. Data Tables **35**, 15 (1986).
[41] K. Pomorski and J. Dudek, Phys. Rev. C **67**, 044316 (2003).
[42] B. G. Carlsson and I. Ragnarsson, Phys. Rev. C **74**, 011302 (2006).
[43] N. Rowley, J. Ollier, and J. Simpson, Phys. Rev. C **80**, 024323 (2009).
[44] S. M. Harris, Phys. Rev. Lett. **13**, 663 (1964).
[45] S. M. Harris, Phys. Rev. **138**, B509 (1965).
[46] J. M. Rees *et al.*, Phys. Rev. C **83**, 044314 (2011).
[47] K. Dusling *et al.*, Phys. Rev. C **73**, 014317 (2006).
[48] R. Janssens, Y. E. Masri, J. M. Ferté, C. Michel, J. Steyaert, and J. Vervier, Nucl. Phys. A **283**, 493 (1977).
[49] A. V. Afanasjev, D. B. Fossan, G. J. Lane, and I. Ragnarsson, Phys. Rep. **322**, 1 (1999).
[50] T. Bengtsson and I. Ragnarsson, Nucl. Phys. A **436**, 14 (1985).
[51] T. Bengtsson, Nucl. Phys. A **512**, 124 (1990).
[52] J. Simpson *et al.*, Phys. Lett. B **327**, 187 (1994).
[53] B. G. Carlsson, I. Ragnarsson, R. Bengtsson, E. O. Lieder, R. M. Lieder, and A. A. Pasternak, Phys. Rev. C **78**, 034316 (2008).
[54] Y. Shi, J. Dobaczewski, S. Frauendorf, W. Nazarewicz, J. Pei, F. Xu, and N. Nikolov (to be published).